DEVELOPMENT OF AN IMPROVED DESIGN PROCEDURE FOR UNBONDED CONCRETE OVERLAYS

TPF-5(269)

Task 3 Report
Structural model development

Prepared by:

Lev Khazanovich
Derek Tompkins

Department of Civil, Environmental, and Geo-Engineering
University of Minnesota

Kevin Alland
John DeSantis
Steven Sachs
Julie Vandenbossche

Department of Civil and Environmental Engineering
University of Pittsburgh

March 2016

CONTENTS

1. PROJECT WORK OVERVIEW

Extensive structural modeling conducted using finite element method (ISLAB2005) to investigate common issues in UBOL

- The structural model explicitly accounts for overlay, interlayer, existing slab, and subgrade support. The joints in the overlay do not necessarily match with joints in the existing pavements. Unlike the AASHTO M-E software, the structural model does not convert the existing and overlay into a single-layer system.
- Models provided insight on effects of damage in existing PCC slab and effects of deterioration near joints.
- Models used to develop thickness relationship between UBOL systems and a single-layer structural equivalent (for a "worse case" scenario that accounts for the presence of distresses in the existing pavement). This relationship can be compared to that of AASHTO93 for a sense of possible outcomes from the new thickness design procedure. An additional benefit of this model is that it can be used to provide a rational approach for the selection of the reduced stiffness of the existing pavement for the AASHTO M-E procedure if this is desirable.
- Structural modeling of six-foot panels was also performed for many case studies. The general finding is that six-foot panel stress concentrations are similar to those of 12-by-15 foot slabs under thermal and single-axle loading.

Structural modeling led to the reconsideration of performance models, including the development of a new joint faulting model

- Transverse bottom-up cracking model can directly account for cracking in the existing pavement. The current AASHTO M-E approach of reducing the existing pavement stiffness can be either improved or replaced altogether.
- Transverse top-down cracking model should be tied with the 3D structural model for joint faulting and the permanent deformation of the interlayer.
- Longitudinal cracking better understood through structural models. While the propagation of longitudinal cracking cannot be addressed, a damage limit can be established based on UBOL design parameters.
- Concerns about reflective cracking have been directly addressed by both the structural modeling and Task 2 work. Generally, limiting damage for the benefit of controlling other distresses will impose sufficient limitations to prevent reflective cracking.
- The joint faulting model will utilize slab faulting response solutions from a three-dimensional finite element structural model currently in development. In addition to guiding the joint faulting model, the 3D structural model will serve other distress models by providing information on the development of deterioration under joints.

Overall the findings of the Task 3 efforts have positioned the research team to advance the design procedure for UBOL, which will be completed in the work of Task 4.

2. STRUCTURAL RESPONSE MODELING OF UNBONDED OVERLAYS OF CONCRETE PAVEMENTS

2.1 Introduction

During Task 3 the research team explored the use of finite element modeling software to develop structure models for the response of unbonded concrete overlays of concrete pavement to loading. Two primary finite element approaches were considered:

- ABAQUS, a commercial software package that has become an industry standard in the development and analysis of sophisticated structural modeling, and
- ISLAB2005, a software package developed by members of the research team exclusively for the response of rigid pavements to loading under a wide variety of standard and non-standard conditions.

While commercial tools such as ABAQUS are fully featured and extremely powerful, they have their drawbacks. In addition to the need for extensive licensing fees, robust software such as ABAQUS also requires extensive user experience to efficiently develop and run structural models. Because ABAQUS caters to engineers across disciplines, it must include a wide variety of features not required by any given user. Navigating these features and narrowing the available tools to those required to – for example – model a pavement is time consuming to the extent of being burdensome. In addition, should a model be set up incorrectly, "on the fly" adjustments are not easy to implement. Finally, ABAQUS requires extensive computational resources and single simulations can take time.

Alternatively, ISLAB2005 presents a more direct, flexible approach, available to the research team through a pre-existing academic license. While, unlike ABAQUS, it is restricted to pavements, its solutions are no less accurate given that ISLAB2005 was developed and tested explicitly for the response of multilayered rigid slabs on grade. Because of this, finite element simulations developed using ISLAB2005 form the basis of the neural networks at the heart of the AASHTO M-E design software. Furthermore, projects can be quickly built and run in ISLAB2005, allowing for more iteration and adjustment than its larger, but no more numerically accurate, commercial alternatives.

2.1.1 Finite element modeling of interlayer behavior in unbonded overlays of concrete pavements

In addition to its flexibility in modeling, ISLAB2005 includes the use of the Totsky model to simulate the interlayer in an unbonded overlay pavement system (Totsky 1981, Khazanovich 1994, Khazanovich and Ioannides 1994). The Totsky assumption is summarized in Figure 1, where the overlay rests on the Totsky spring interlayer and the existing slab rests on a Winkler subgrade.

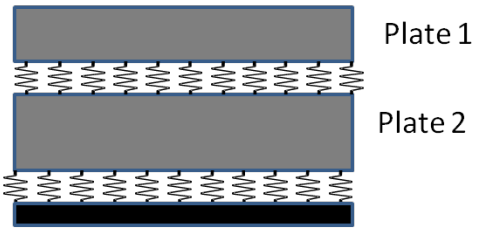

Figure 1. Totsky model for layer interface in UBOL system adopted in ISLAB2005

The advantage of the Totsky model is that it can model the "cushioning" property of the interlayer in a straightforward, computationally efficient manner. The Totsky model was specifically implemented in ISLAB2005 to model unbonded concrete overlays. Similarly, a Totsky approach could also be implemented in larger commercial FEM packages; as noted previously, the implementation of this approach is time consuming given the extent of features available and the relative difficulty in their implementation.

As the Totsky approach is able to be adopted without any additional complication in ISLAB2005 projects, the majority of the work of Task 3 utilized ISLAB2005 for its finite element modeling of UBOL structures. Doing so allowed the research team to investigate many combinations of varied support conditions, loading conditions, layer properties, and interlayer properties in modeling the response of the UBOL system, as detailed in the subsections to follow. In addition, the use of ISLAB2005 does not preclude the later use of the other commercial FEM packages; rather, ISLAB2005 is used for the initial structural modeling, and if more sophisticated three-dimensional models are required, they can be developed and adopted at a later time.

2.2 Using laboratory reflective cracking beams to develop interlayer parameter for structural model

2.2.1 Modeling a relationship between Totsky coefficients and beam response

There were tests conducted during the laboratory work of Task 2 that can be used for the Totsky vertical stiffness coefficient. Those tests are "Deflection Characterization" and "Reflective Cracking," using the terms applied in the Task 2 final report. The work of Task 3 initially investigated the use of data from both tests. Eventually the research team focused exclusively on the Reflective Cracking test, as it is easier to analyze mechanically in ISLAB2005 for the benefit of the Totsky approach. (The Deflection Characterization test and related data may be revisited in later stages of the project work should the need arise.) The following section details the understanding of the Reflective Cracking test configuration that was modeled using the finite element approach implemented in ISLAB2005.

The laboratory beam specimen used for the "Reflective Cracking" tests of Task 2 is presented in Figure 2. Specifics of the beam are:

- The composite beam (of three layers) is 30 inches in length and 6 inches in width
- The top layer of the beam is a PCC layer of depth 6 inches with modulus that varies depending on specimen (roughly 4,000,000 psi).

- The interlayer is either a HMA or fabric interlayer.
- The bottom layer is an existing PCC layer of thickness 6 inches with variable modulus (roughly 4,000,000 psi)
- The bottom layer contains a notch through the depth and thickness of the layer. The notch is located at mid-span of the beam. The notch simulates an in-situ crack.

In the Task 2 "Reflective Cracking" test configuration, there were no restraints on either the top or the bottom layer. The beam was supported under mid-span 10 inches from either end using a neoprene pad with effective k-value of 200 psi/in. Thus, the middle third of the beam, centered under the load, is unsupported. Finally, the beam was loaded on the surface of the top layer at mid-span, directly over the crack/notch. In the lab, the load rate was 30 pounds per second, applied until failure in the top layer.

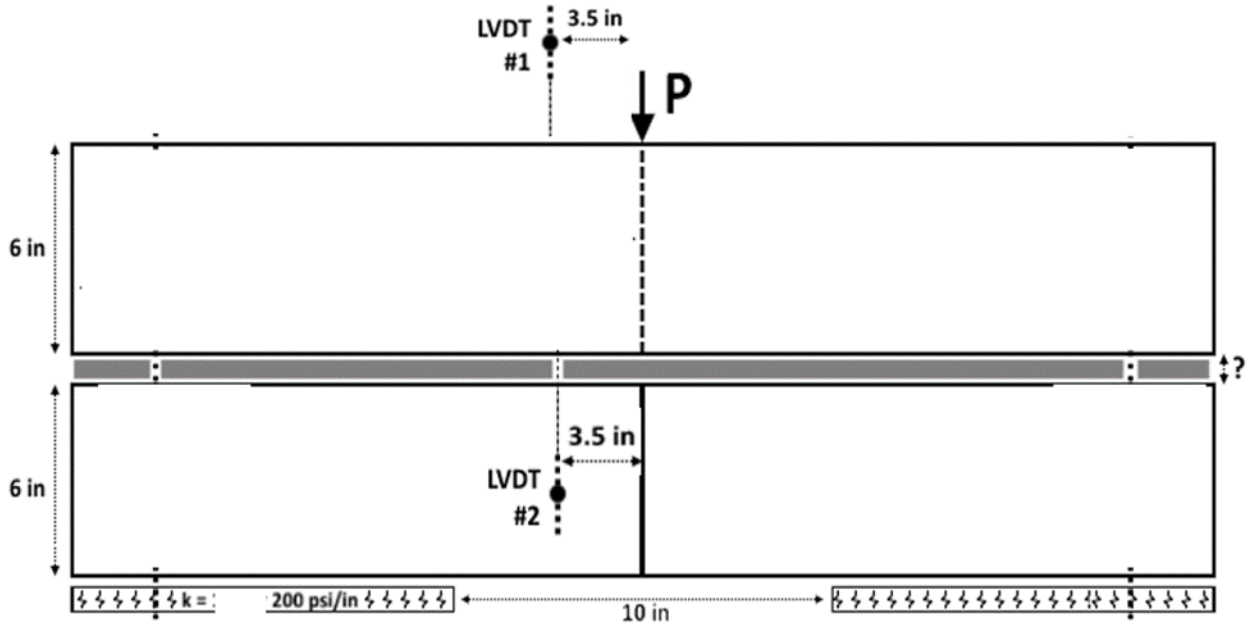

Figure 2. Laboratory beam specimen for reflective crack testing

As noted in Section 2.1, given that ISLAB2005 uses the Totsky approach for interlayer behavior in overlays of existing PCC pavements, reproducing the Task 2 beam from Figure 2 in a finite element model is relatively straightforward. A representation of the model is illustrated in Figure 3. Note that the simulated load is applied as a one-inch wide line-load along the beam depth of 6 inches (indicated in blue in Figure 3a and Figure 3b). Thus, the load contact area is 6 in^2. As the finite element model is static, a single load of 1 kip is applied to determine a linear response of the beam model to loading.

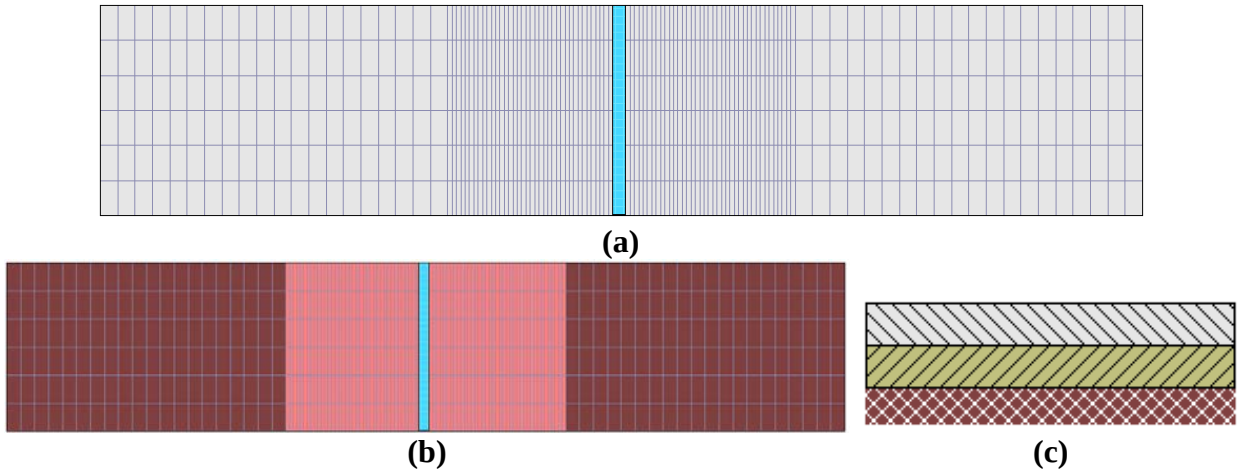

Figure 3. ISLAB2005 two-dimensional model of reflective cracking beam from Task 2 lab study: (a) full mesh in plan view; (b) example of lack of support under span in pink in plan view; (c) cross-section of multi-layered system (through thickness)

One non-trivial need for the model is the need to represent the notch in the lab beam. Fortunately, the finite element software is able to simulate this without issue. In ISLAB2005, the notch/crack is effectively modeled by inserting a fictitious "joint" at mid-span. In the upper layer (the overlay), this joint fully transfers load (i.e. the load-transfer efficiency is 100%). However, I in the lower layer (the existing PCC), the joint is does not transfer the load at all (i.e. load transfer efficiency is near-zero). This modification allows the simulations to consider the notch without any model complications or special conditions. The simulations were verified through multiple stages of review by the research team. An example of a Task 2 beam response to a 1-kip load at mid-span is provided in Figure 4.

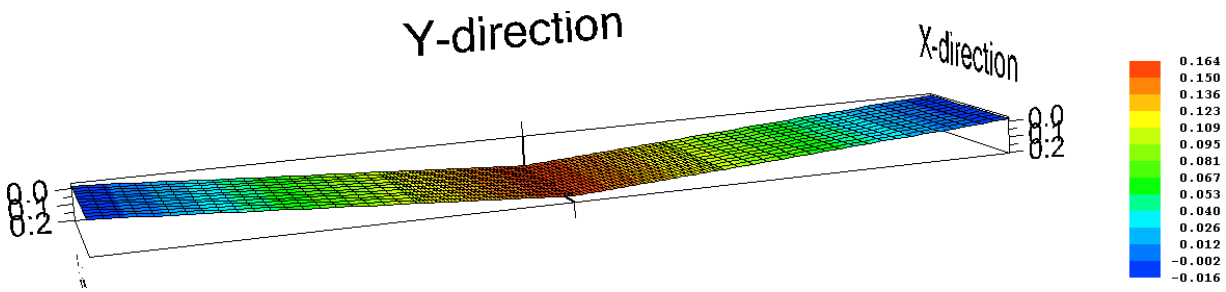

Figure 4. Example of upper layer deflection from ISLAB2005 results for simulated Task 2 reflective cracking beams

Given a Task 2 beam model that the research team felt confident in, the project work then involved developing a factorial of cases to model the response of beams utilizing interlayers of different properties. The cases vary only in the Totsky interlayer coefficient (k_{totsky}) assumed, otherwise the modeled beam has the properties:

- Layer 1: h_{OL} = 6 in, E_{OL} = 4,255,000 psi (average of all Task 2 beam overlay elastic moduli), Poisson ratio ν = 0.15, unit weight γ = 0.087 lb/in^3
- Interlayer: k_{totsky} varied from 10 to 50,000 pci

- Layer 2: h_{OL} = 6 in, E_{OL} = 4,790,000 psi (average of all Task 2 beam existing PCC elastic moduli), Poisson ratio ν = 0.15, unit weight γ = 0.087 lb/in^3
- Mesh details: Mesh elements are square (0.5 inches to a side) 10 inches or more away from load. In the 10-inch region centered on mid-span, mesh elements are refined to a dimension of 0.5 by 0.125 inches, as illustrated in Figure 3a.
- A static load of 1-kip is applied to determine a linear beam response associated with interlayer properties.

Figure 5 illustrates the final relationship determined for the modeled beam response and Totsky interlayer coefficient. Also included in the figure is an exponential relationship determined by transforming the variables and finding a linear least-squares fit. As shown in the figure, the R-squared valued for the fitness of the exponential relationship is 0.9975, thus the research team is confident that it adequately describes the relationship between model response and Totsky coefficient for this range of coefficient values.

Thus, given the relationship in Figure 5, the research team was prepared to infer Totsky interlayer coefficients from the Task 2 "Reflective Cracking" beam data. Those efforts are summarized in the following subsections for beams with fabric interlayers and beams with HMA interlayers, respectively.

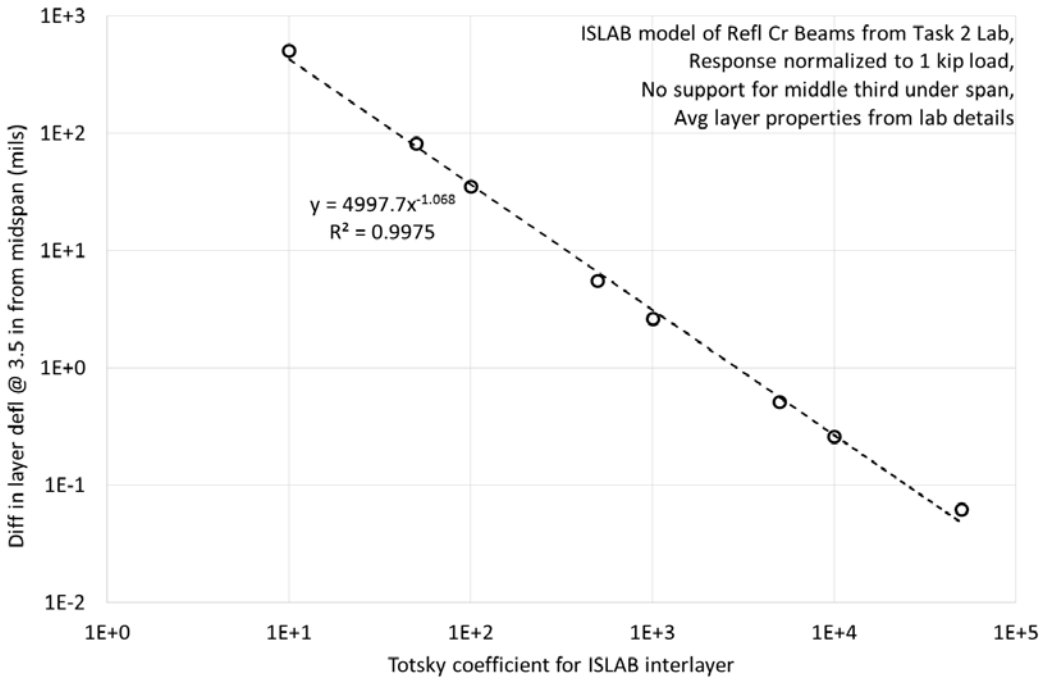

Figure 5. Developed relationship between difference in layer deflection (in mils) and Totsky spring coefficient for interlayer from finite element simulations conducted using ISLAB2005

2.2.2 Fabric interlayer beam response

Of the tests conducted during Task 2 involving fabric interlayers, four were deemed acceptable to use for analysis. These beams are described in Table 1 below.

Table 1. Details of Task 2 reflective cracking beams with fabric interlayer, including beam response at 1 kip load and associated Totsky spring coefficient from finite element simulations

Existing PCC				Overlay PCC				Fabric Type	dW @ 1 kip (mils)	ISLAB Totsky Coefficient
Specimen	E (psi)	f'c (psi)	MOR (psi)	Specimen	E (psi)	f'c (psi)	MOR (psi)			
0409F10EA	4600000	6982	863	0501F10OA	4170000	5069	641	F10	7.76	560.3
0302F15EB	4800000	6991	905	0701F15OD	4430000	4632	682	F15	12.33	341.6
0406F15EC	4640000	6982	884	0429F15OC	4280000	5059	644	F15	10.41	409.6
0406F15EB	4640000	6982	884	0429F15OB	4280000	5059	610	F15	5.46	816.3

Given the response of the fabric beams under a 1-kip load in the lab, the modeled relationship was used to infer an associated Totsky interlayer coefficient. The coefficients determined are illustrated in Figure 6 for comparison – the exact inferred coefficient for each beam is indicated in the right-most column of Table 1.

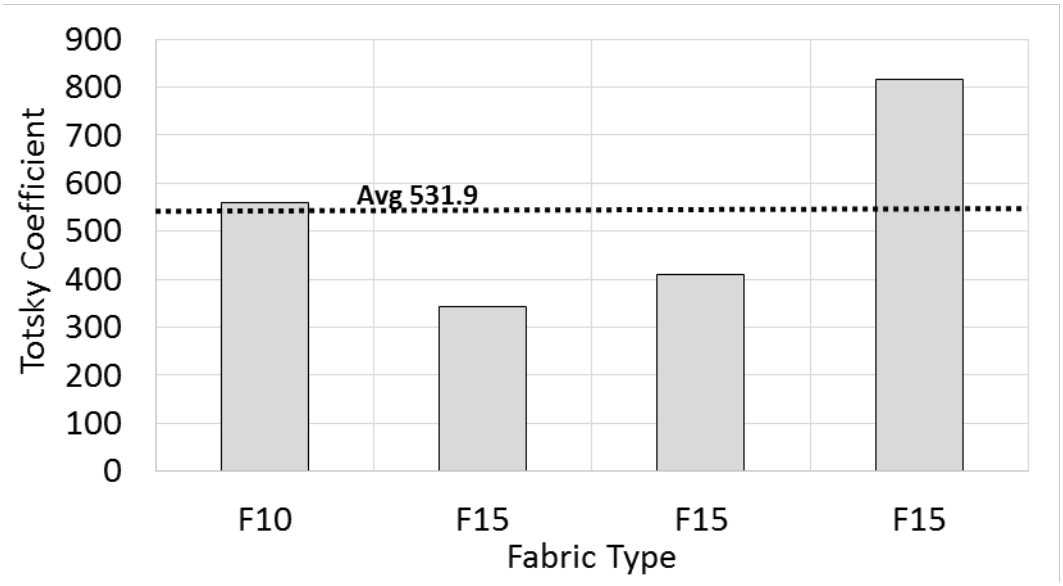

Figure 6. Totsky spring coefficient values associated with responses of Task 2 reflective cracking beams with fabric interlayers

2.2.3 HMA interlayer beam response

Of the HMA interlayer beams from the laboratory work of Task 2, a total of 12 were used in the analysis. These beams are described in Table 2 below.

Table 2. Details of Task 2 reflective cracking beams with HMA interlayer, including beam response at 1 kip load and associated Totsky spring coefficient from finite element simulations

Specimen	Dense or Open Graded	Aged or New	Unmilled or Milled	E (psi)	f'c (psi)	MOR (psi)	Avg HMA thickness (in)	dW @ 1 kip (mils)	ISLAB Totsky coefficient (pci)
0417MNDAUA	D	A	U	3880000	4590	590	2.9	0.93	5371.9
0701MNDAUA	D	A	U	4430000	4632	658	2.8	0.76	6686.0
0507MNDAUA	D	A	U	4480000	5106	738	2.8	2.32	2036.2
0520MIOAUC	O	A	U	4620000	5073	711	1.9	0.68	7602.6
0701MNONUB	O	N	U	4430000	4632	636	1.8	2.30	2058.0
0513MIOAUC	O	A	U	4710000	5013	697	1.8	1.28	3844.8
0522MNONUC	O	N	U	4650000	5131	724	1.7	0.93	5393.4
0909PADNUC	D	N	U	4340000	4824	656	1.5	0.63	8161.8
0909PADNUA	D	N	U	4340000	4824	641	1.4	1.30	3766.9
0424MIDAUC	D	A	U	4230000	5106	652	1.1	0.46	11408.0
0507MNDAMB	D	A	M	4480000	5106	690	1	1.25	3928.8
0515MIDAUB	D	A	U	4790000	5131	717	1	0.13	43875.7

Given the response of the HMA beams under a 1-kip load in the lab, the modeled relationship was used to determine an associated Totsky interlayer coefficient. The coefficients determined are illustrated in Figure 7 for comparison – the exact inferred coefficient for each beam is indicated in the right-most column of Table 2. Note that the beam designated 0515MIDAUB – listed in the last row of Table 2 – has been excluded from analysis as an outlier.

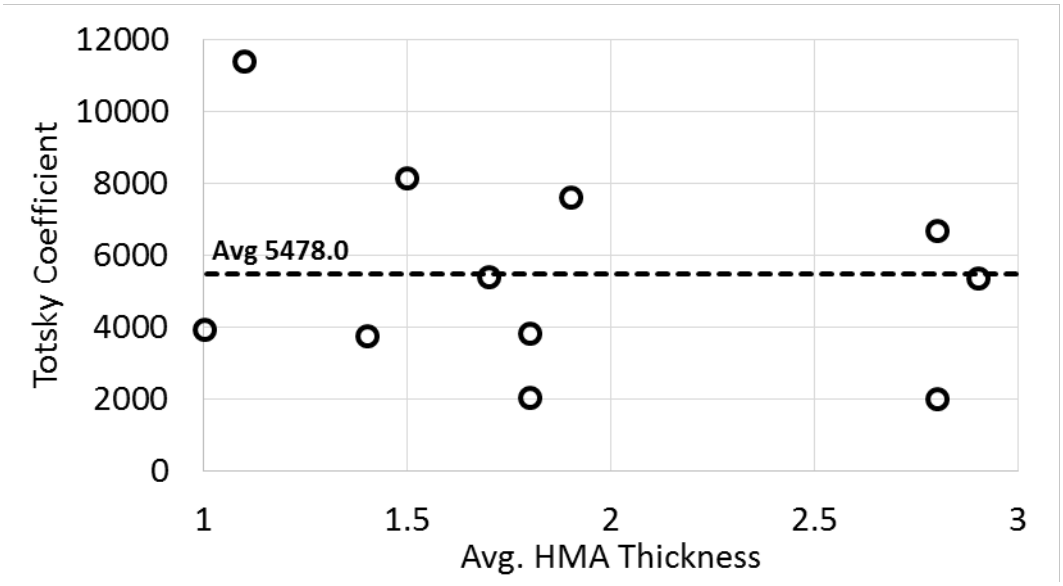

Figure 7. Totsky spring coefficient values associated with responses of Task 2 reflective cracking beams with HMA interlayers

Note that there does not appear to be a relationship between interlayer HMA thickness and the inferred Totsky coefficient. Based on the model and the lab data, other factors, including

interlayer bond and perhaps loading/support conditions, must be considered if the inferred Totsky coefficient is to be considered beyond an average across all HMA lab beams.

2.3 Determining single-layer structural equivalence for unbonded systems using finite element modeling and Totsky approach for the interlayer

2.3.1 Methodology

Given a working estimate of appropriate Totsky interlayer coefficients based on the developed finite element models and the Task 2 laboratory experiments, the research team developed a series of finite element projects (using ISLAB2005) to understand UBOL slab behavior relative to single-layer slab behavior. The created projects in total represent 11 systems:

- Nine single-layer projects, for slab thickness of 7 inches to 15 inches in one-inch increments,
- One two-layer project for a 7-inch overlay (Layer 1) on an existing 10-inch slab (Layer 2)
- One two-layer project for a 10-inch overlay (Layer 1) on an existing 7-inch slab (Layer 2)

Other shared features across all projects are:

- All developed projects used identical meshes and slab dimensions, 12 feet by 12 feet. The slab mesh is illustrated in Figure 8. The mesh elements have dimensions of 6-inch on either side except for those elements within 12 inches of either the slab edge or the underlying crack at midslab of the system. In that case mesh element are sized 1-inch along the dimension perpendicular to the slab edge or crack.
- Default ISLAB2005 layer properties for PCC (Layer 1) in all projects
- Default subgrade response for all projects
- In UBOL projects…
    - Assume Totsky approach with vertical stiffness of 5478 (average of HMA interlayer values from Table 2).
    - Layer 2 assumes default ISLAB2005 properties for PCC, identical to those used for Layer 1
    - A rigid joint is assumed for Layer 1, and a discontinuous joint (with LTE of 1%) is assumed for Layer 2 to simulate a crack in the existing slab at mid-slab. This assumption is the same as the assumed condition for the existing layer in the finite element simulations used to investigate the Totsky interface coefficients.

The developed projects were subjected to three loading conditions:

- A 9-kip “point load” applied in a 562.5 psi region,
- A standard 18-kip single-axle load, and
- A standard 18-kip single-axle load with a positive 15°F linear thermal gradient through the thickness of Layer 1.

The two load types (point load and single axle) are illustrated in Figure 8.

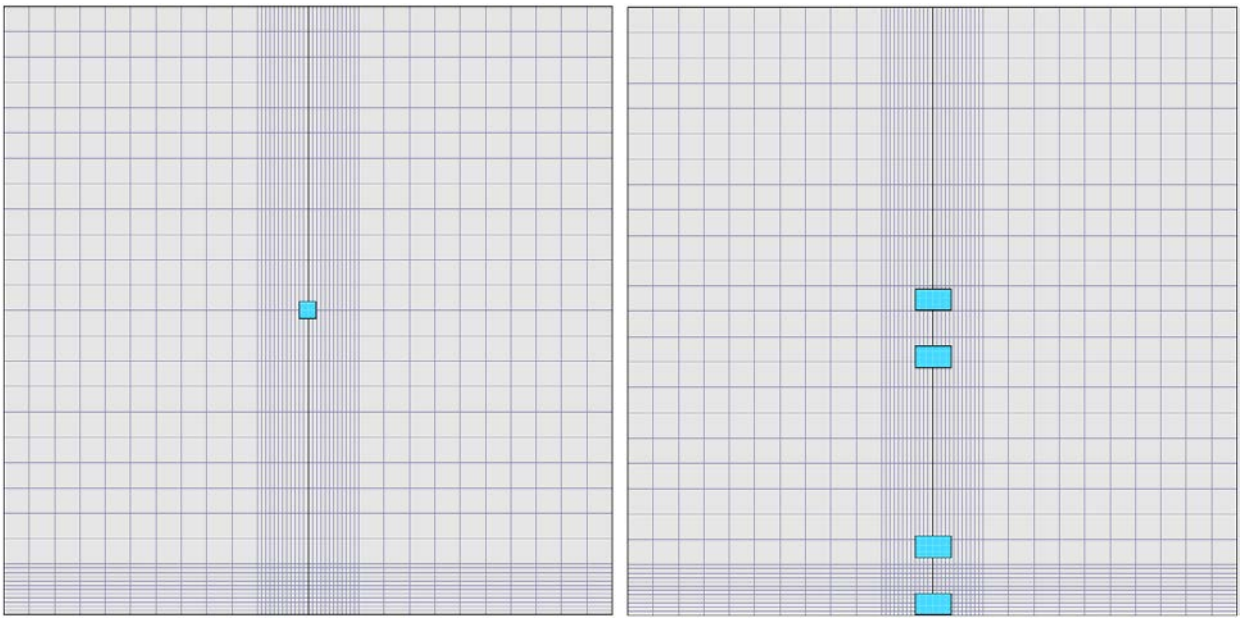

(a) **(b)**

Figure 8. Finite element mesh in ISLAB2005 and a) fictitious point load and b) standard single-axle load configurations used for simulations

2.3.2 Investigation using finite element simulations

Results of the developed simulations discussed above are summarized in Figure 9 through Figure 11, where each figure describes the stress response of single-layer slabs and UBOL to:

- A 9-kip point load (Figure 9),
- A standard 18-kip single axle load (Figure 10), and
- A standard 18-kip single-axle coupled with thermal loading conditions (Figure 11).

Each figure contains two pairs of related subfigures with the following characteristics. The first pair of subfigures illustrates the stress state in the pavement systems:

- Subfigure "a" describes the stress at the bottom of Layer 1 in the *y*-direction (the direction of travel) along the longitudinal direction for the entire modeled system.
- Subfigure "b" describes the stress at the bottom of Layer 1 in the *y*-direction (the direction of travel) along the longitudinal direction within a two-foot region centered on mid-slab (where the crack occurs in the existing PCC layer).
- In subfigures "a" and "b," the legend indicates the single-layer (1L) and two-layer (2L) systems and their thicknesses accordingly. For example, "1L_8" refers to a single-layer system with slab thickness of eight inches.

The second pair of subfigures compares the performance of the slabs to more directly assess the issue of structural equivalence.

- Subfigure "c" describes the maximum stress response, σ_{max}, given single-layer PCC thickness. Also charted in this subfigure is the maximum stress response for the two UBOL systems, indicated with a line and label.
- Subfigure "d" describes the average stress response, σ_{avg}, given single-layer PCC thickness across a region within 8 inches of the load (applied at mid-slab). Also charted in this subfigure is the average stress response across an identical region in the two UBOL systems, indicated with a line and label.

Thus, in comparing these two pairs of subfigures across the three loading conditions, one can see that as the severity of the load increases, the stress in the slab increases accordingly. While not unexpected, this validates that the approach provides rational results, at least to the extent of the cases considered.

More importantly, within each figure one is able to identify the performance of UBOL relative to single-layer systems. For instance, using Figure 9b as an example, one can see how the stress behavior in UBOL differs from that of single-layer systems under load; more precisely, in UBOL the stress gradient is more exaggerated in the "worst case" load location for UBOL, when the load occurs directly over the crack in the existing PCC.

In addition, using Figure 9c, one can see that a 9-kip point load induces a peak stress of 351 psi in a 7-inch single-layer system and a peak stress of 325 psi in a 7-on-10 inch UBOL. Likewise, using Figure 11c, one can see that an 18-kip single-axle and thermal load induces a peak stress of over 500 psi (512 psi) in a 7-inch single-layer system and a peak stress of 427 psi in a 7-on-10 inch UBOL.

A final comparison using the figures is to raise the appropriateness of using σ_{max} to determine structurally equivalent behavior in this work. Instead, as noted previously, the research team averaged the stress across a 16-inch wide region centered on the load to develop a σ_{avg} value for each system. Using σ_{avg} to approximate structural equivalency among the systems, the simulations indicate that for the 18-kip single-axle, thermally loaded instance:

- a 7-on-10 UBOL system responds similarly to an 8-inch single-layer slab and
- a 10-on-7 UBOL system responds similarly to a 10.5-inch single-layer slab.

The consideration of structural equivalence is important in the design and performance of UBOL. As the use of σ_{max} may underestimate the structural equivalence of UBOL to single-layer systems, the value of σ_{avg} can be also understood as preventing overly conservative overlay thickness design.

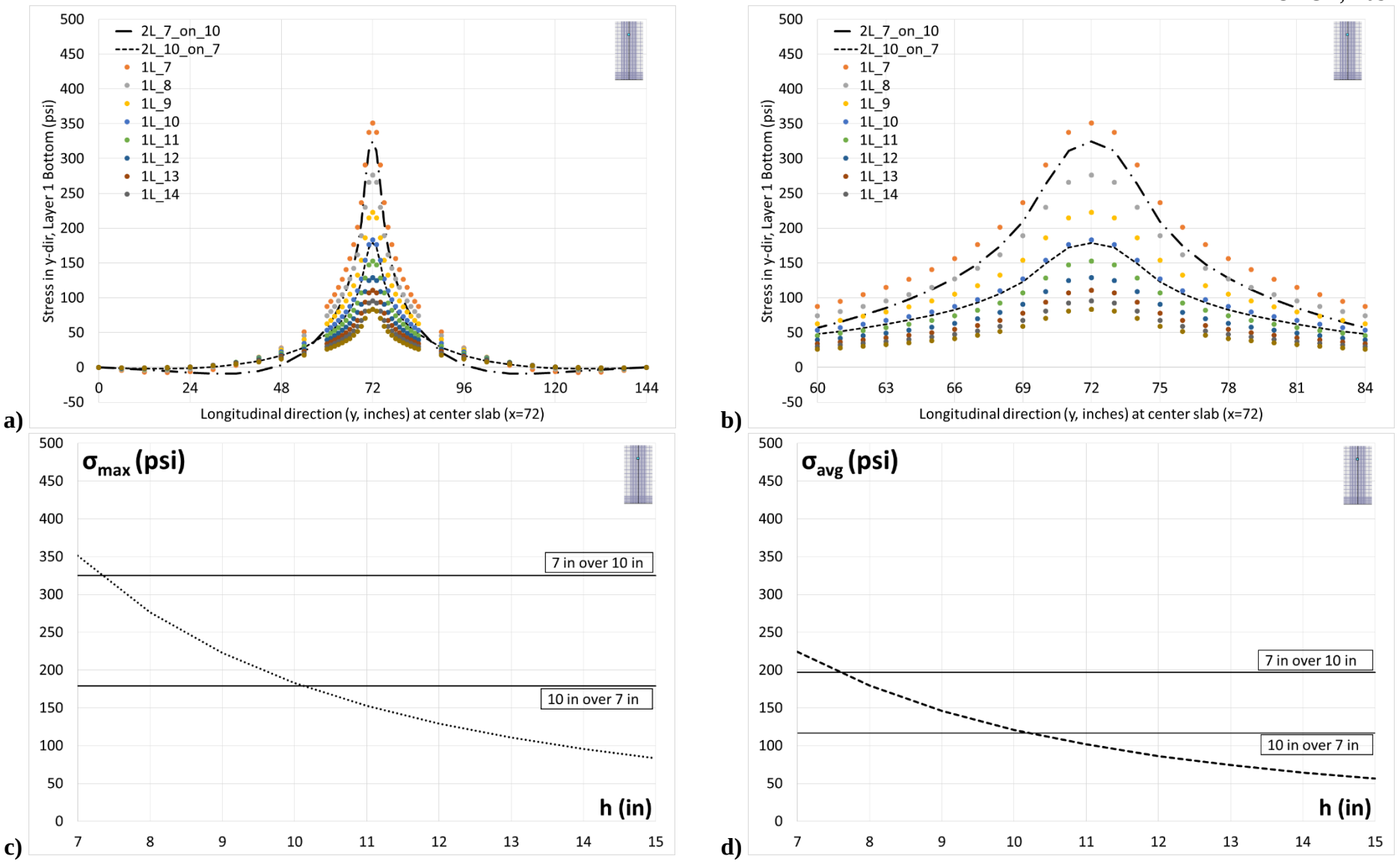

Figure 9. Response of two-layer and single layer systems to 9-kip "point load" at slab center in (a) full slab and (b) in 2-foot region centered on discontinuity in existing PCC; UBOL and single-layer slab equivalency for (c) maximum stress at slab edge given point load and (d) average stress across a two-foot length centered on discontinuity in existing layer under point load

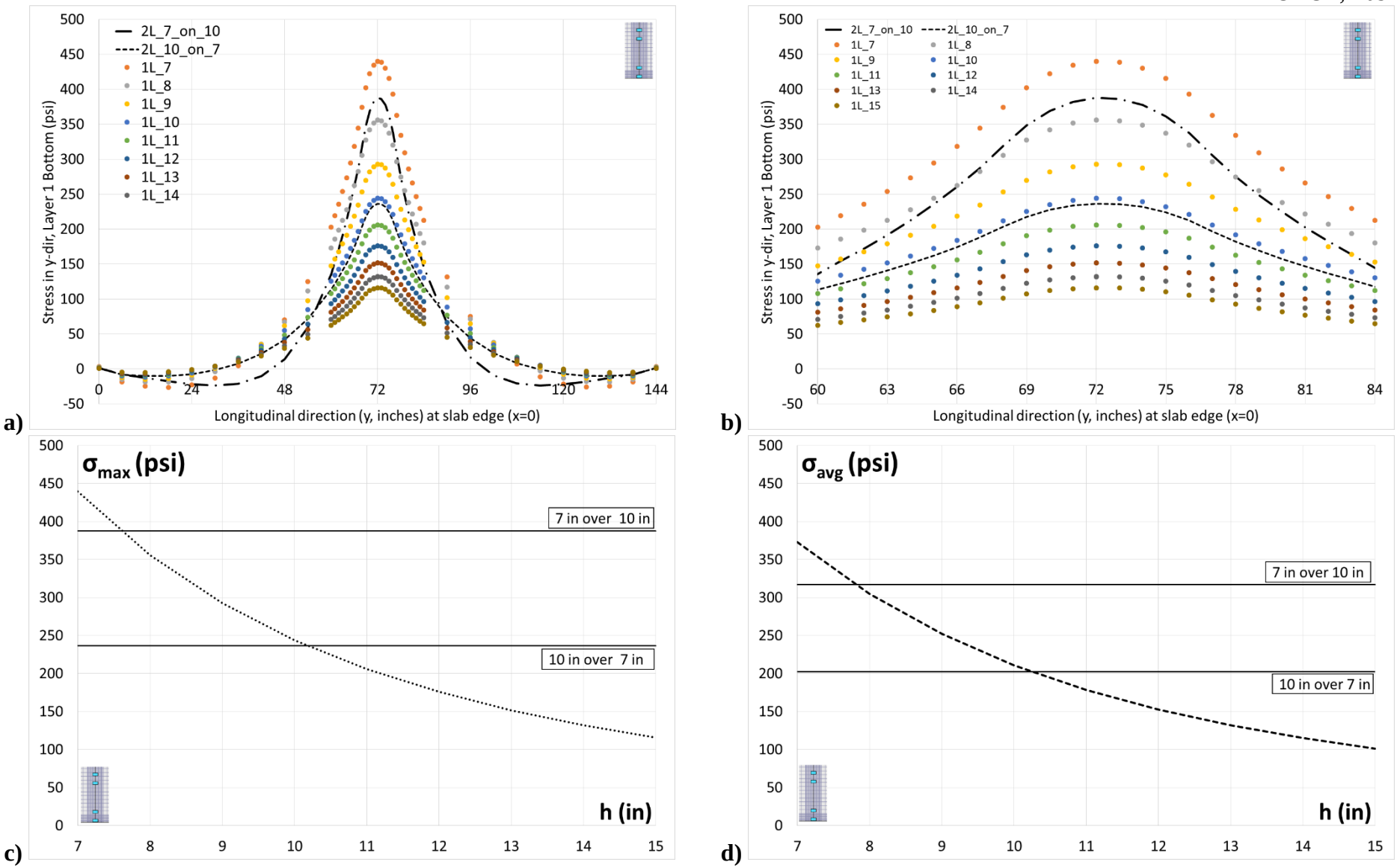

Figure 10. Response of two-layer and single-layer systems to 18-kip single axle load in (a) full slab and (b) in 2-foot region centered on discontinuity in existing PCC; UBOL and single-layer slab equivalency (c) maximum stress at slab edge given 18-kip axle load and (d) average stress across a two-foot length centered on discontinuity in existing layer under axle load

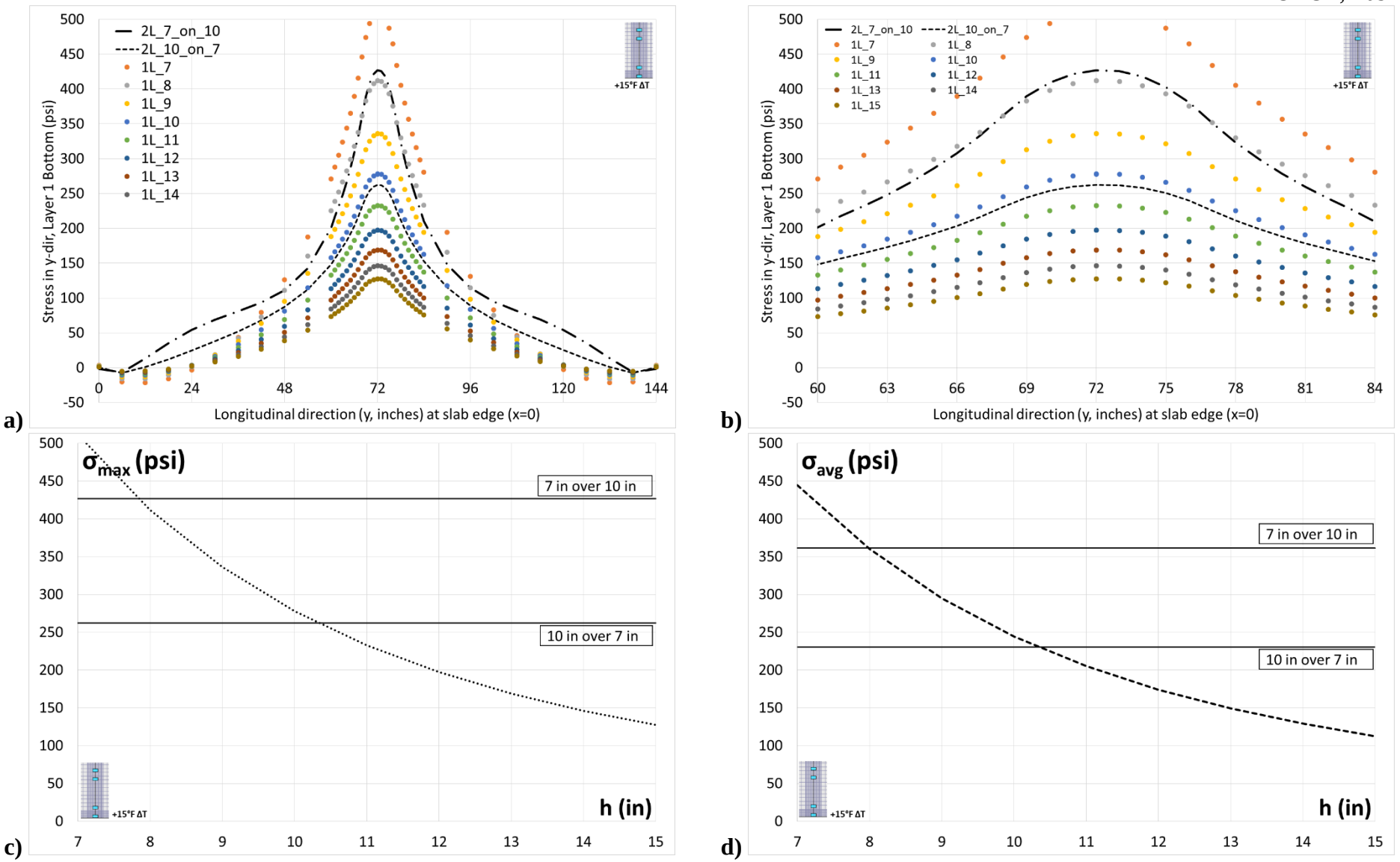

Figure 11. Stress response of two-layer and single layer systems to 18-kip axle load and linear thermal gradient in (a) full slab and (b) in 2-foot region centered on discontinuity in existing PCC; UBOL and single-layer slab equivalency (c) maximum stress at slab edge given axle/thermal load and (d) average stress across a two-foot length centered on discontinuity in existing layer under axle/thermal load

2.3.3 Relating UBOL structural response to single-layer PCC slab response for worst-case scenario

Given the results of the final investigation in Section 2.3.2, involving an 18-kip single-axle load and positive thermal gradient, the research team developed a full series of ISLAB2005 simulations to determine the structural equivalence for UBOL systems relative to that of single layer systems. 139 projects were created to represent 11 single-layer PCC systems and 128 UBOL systems:

- Single-layer projects were created for varying slab thickness, from 5 inches to 15 inches in one-inch increments;
- 64 two-layer projects with a Totsky interlayer coefficient of 532 (simulating a fabric interlayer, see Table 1) were created for variable overlay (Layer 1) and existing PCC slab (Layer 2) thicknesses, both having values from 5 to 12 inches in one-inch increments; and
- 64 two-layer projects with a Totsky interlayer coefficient of 5478 (simulating an HMA interlayer, see Table 2) were created for variable overlay (Layer 1) and existing PCC slab (Layer 2) thicknesses, both having values from 5 to 12 inches in one-inch increments.

Other shared features across all projects are:

- All developed projects used identical meshes and slab dimensions, 12 feet by 15 feet. (Note that the slab dimensions were modified from the investigation described in Section 2.3.2.)
- The slab mesh is illustrated in Figure 12b. The mesh elements have dimensions of 6-inch on either side except for those elements within 18 inches of either the slab edge or the underlying crack at midslab of the system. In that case mesh element are sized 1-inch along the dimension perpendicular to the slab edge or crack. (The mesh is more refined than the mesh used in Section 2.3.2.)
- Layer 1 elastic modulus is 4,790,000 psi, an average of the existing PCC modulus from the Task 2 beams discussed above. All other Layer 1 properties are ISLAB2005 defaults, as detailed above.
- Subgrade response of 200 psi for all projects.
- In UBOL projects, the Layer 2 elastic modulus is 4,255,000 psi, an average of the overlay PCC modulus from the Task 2 beams discussed above. All other properties are identical to those of Layer 1.
- In UBOL projects, a rigid joint is assumed for Layer 1, and a discontinuous joint (with LTE of 1%) is assumed for Layer 2 to simulate a crack in the existing slab at mid-slab.
- All systems use a standard 18-kip single-axle load at the slab edge with a positive 15°F linear thermal gradient as the loading condition. Thus the critical stress location, given the orientation of the load and the underlying crack in UBOL systems, is mid-slab in the *y*-direction (longitudinal) at the transverse slab edge.

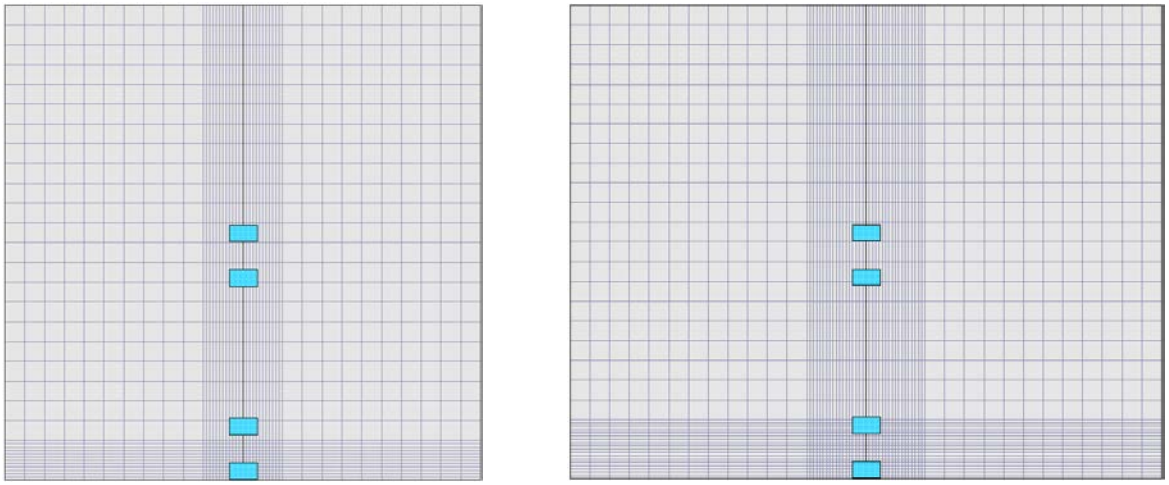

(a) **(b)**

Figure 12. Single-axle load shown on finite element mesh in ISLAB2005 used for a) 12-foot by 12-foot slab in initial investigation and b) 12-foot by 15-foot slab for full structural response comparison

The final results of the 139 simulations are illustrated across two figures:

- Figure 13 compares the average stress response (σ_{avg}, calculated for a region within 18 inches of the critical stress location along the slab edge) for overlay systems with an HMA interlayer and single-layer systems. Here each colored line represents the response of a system with fixed overlay thickness with variable underlying existing PCC thickness (h_{PCC}), and the black line represents the response of a single-layer system with variable PCC thickness (h_{PCC}).
- Figure 14 compares the σ_{avg} for overlay systems with fabric interlayers, with all other figure properties identical to those of Figure 13.

There are a number of observations that can be made on these two figures. For instance, systems with HMA interlayers receive see a greater stress reduction given thicker existing slabs than do systems with fabric interlayers. Also, for identical overlay and existing slab thicknesses, the HMA interlayer appears to provide much more structural benefit than a fabric interlayer, e.g. a 6-inch overlay on 9-inch existing slab with an HMA interlayer performs similarly to an 8-inch single-layer PCC, whereas the same UBOL system with a fabric interlayer has a response similar to a 6.75-inch single-layer PCC.

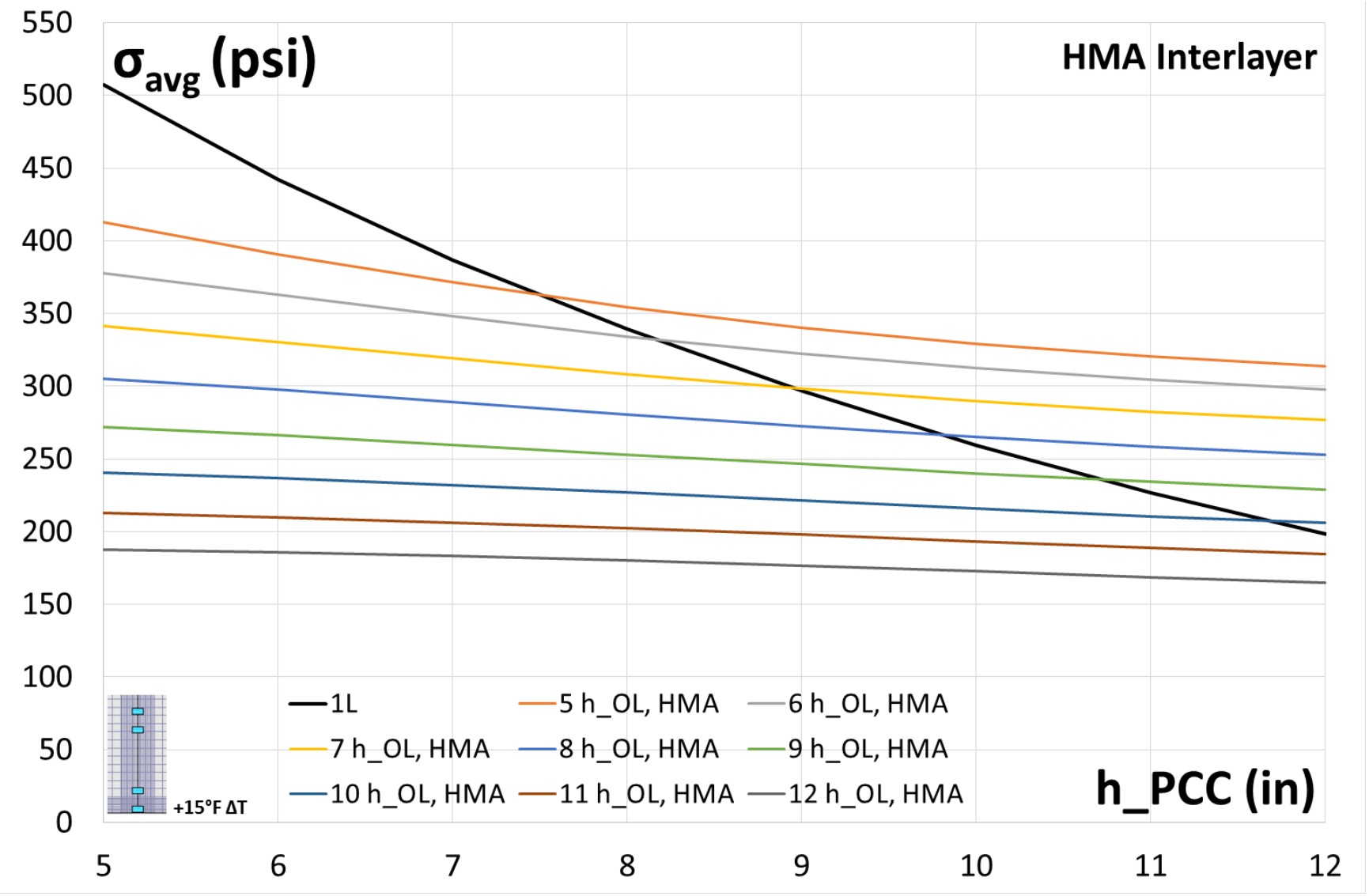

Figure 13. Structural response of UBOL systems with HMA interlayer (each colored line corresponds an overlay thickness with underlying h_{PCC} thickness) relative to single-layer slab performance (with thickness h_{PCC})

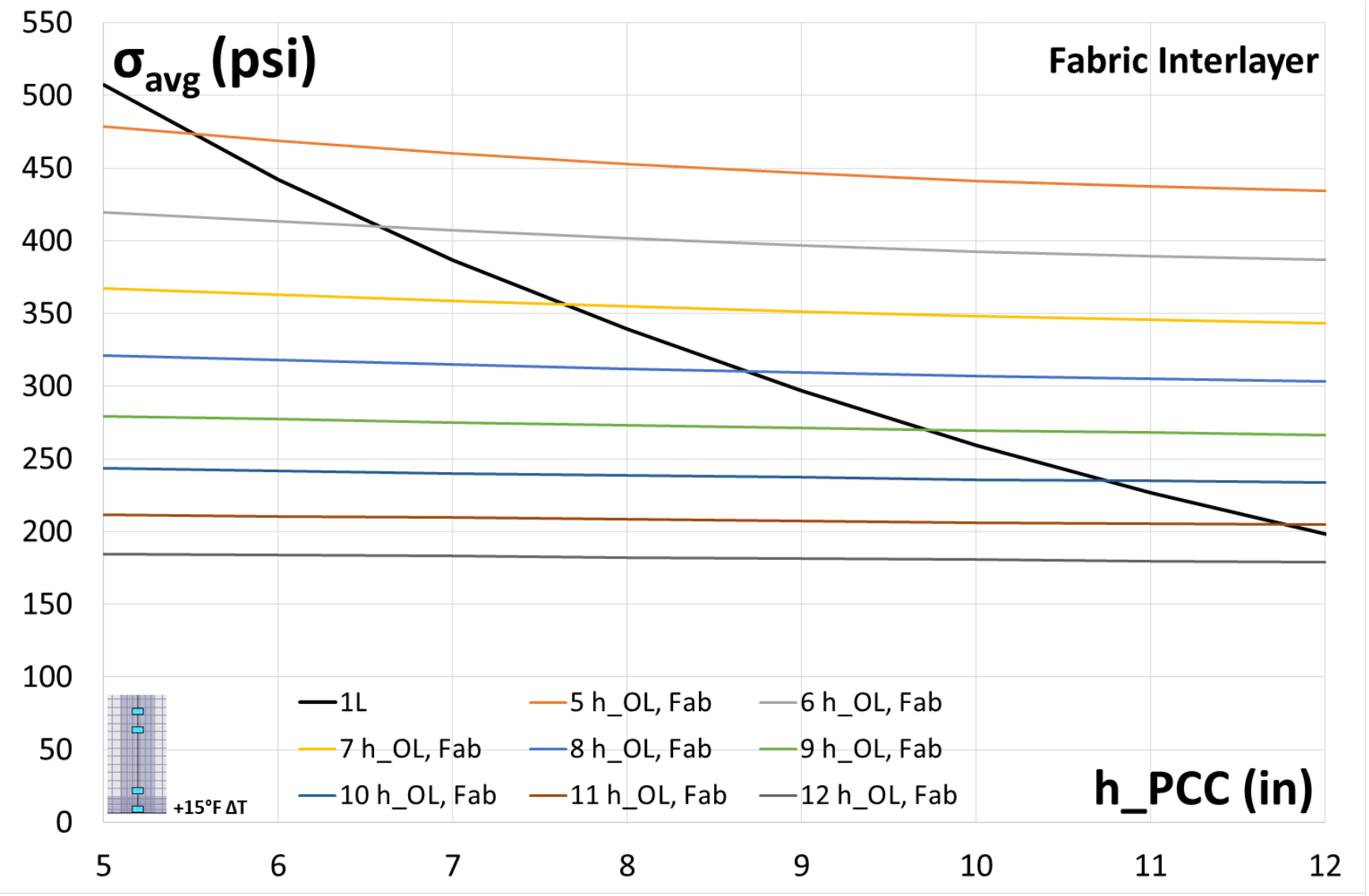

Figure 14. Structural response of UBOL systems with fabric interlayer (each colored line corresponds an overlay thickness with underlying h_{PCC} thickness) relative to single-layer slab performance (with thickness h_{PCC})

2.3.4 Comparing developed structural equivalence estimates with those of AASHTO 1993 for unbonded overlay designs

Finally, the structural equivalence using stress response in Figure 13 and Figure 14 can be compared with other methods of estimating structural equivalence, most notably the design method discussed in the AASHTO 1993 Design Guide. This method can be summarized by an equation that produces an effective single-layer equivalent to a designed unbonded overlay

$$h_{eff} = \sqrt{h_{OL}^2 + C_{ex} h_{PCC}^2} \quad (1)$$

where h_{eff} is the single-layer slab equivalent, h_{OL} is the thickness of the design unbonded overlay, h_{PCC} is the thickness of the existing PCC slab, and C_{ex} is the condition factor for the existing slab, which has a default value of 0.35 and can vary from 0 to 1. Table 3 and Table 4 compare the structural equivalence estimates for systems with HMA and fabric interlayers, respectively. The analysis assumes the AASHTO default for C_{ex}. The tables report a subset of the full finite element projects where h_{OL} is between 6 and 12 inches and h_{PCC} is 6 or 12 inches.

The first observation that can be made is that the AASHTO 1993 structural equivalence overestimates the structural contribution of h_{PCC}, even when the default value of C_{ex} is used. For the two estimates to agree, a lower value of C_{ex} would have to be selected for systems with thicker values of h_{PCC}. Also, it appears that the two estimates of structural equivalence disagree on the contribution of h_{OL} in thinner systems (i.e. those where h_{OL} is less than 8 or 9 inches). However, this difference is indirectly tied back to the consideration of h_{PCC} and C_{ex}.

The finite element systems in these tables assume the worst possible case for the UBOL, wherein a crack in the existing slab is located directly under the load and the system is subjected to a thermal gradient. Thus, with less extreme loading conditions in place, the difference between the two structural equivalence estimates would widen.

However, ***agreement is not the aim of this comparison***. Rather, the comparison calls attention to C_{ex}. C_{ex} is the AASHTO 1993 approach to an important concept for design: accounting for the structural influence of existing damage in the PCC slab to be overlaid. To this end, the finite element simulations conducted in Task 3 can be expanded to investigate the performance of existing slabs and better represent the concept of C_{ex}.

Table 3. Equivalent thicknesses given finite element HMA interlayer project results and AASHTO 1993 unbonded design estimation

HMA Project	h_{OL} (in)	E_{OL} (psi)	k_{totsky}	h_{PCC} (in)	E_{PCC} (psi)	σ_{max} (psi)	σ_{avg} (psi)	h_{eff} (in)	
								AASHTO 1993	ISLAB/ TPF(5)-269
H_06_06	6	4.26E+6	5.48E+3	6	4.79E+6	584	363	7.0	7.5
H_06_12	6	4.26E+6	5.48E+3	12	4.79E+6	498	298	9.3	9.0
H_07_06	7	4.26E+6	5.48E+3	6	4.79E+6	496	331	7.8	8.2
H_07_12	7	4.26E+6	5.48E+3	12	4.79E+6	427	277	10.0	9.5
H_08_06	8	4.26E+6	5.48E+3	6	4.79E+6	426	298	8.8	9.0
H_08_12	8	4.26E+6	5.48E+3	12	4.79E+6	369	253	10.7	10.2
H_09_06	9	4.26E+6	5.48E+3	6	4.79E+6	368	266	9.7	9.8
H_09_12	9	4.26E+6	5.48E+3	12	4.79E+6	321	229	11.5	10.9
H_10_06	10	4.26E+6	5.48E+3	6	4.79E+6	319	237	10.6	10.7
H_10_12	10	4.26E+6	5.48E+3	12	4.79E+6	280	206	12.3	11.7
H_11_06	11	4.26E+6	5.48E+3	6	4.79E+6	278	210	11.6	11.6
H_11_12	11	4.26E+6	5.48E+3	12	4.79E+6	245	184	13.1	12.6
H_12_06	12	4.26E+6	5.48E+3	6	4.79E+6	243	186	12.5	12.5
H_12_12	12	4.26E+6	5.48E+3	12	4.79E+6	216	165	13.9	13.4

Table 4. Equivalent thicknesses given finite element fabric interlayer project results and AASHTO 1993 unbonded design estimation

Fabric Project	h_{OL} (in)	E_{OL} (psi)	k_{totsky}	h_{PCC} (in)	E_{PCC} (psi)	σ_{max} (psi)	σ_{avg} (psi)	h_{eff} (in)	
								AASHTO 1993	ISLAB/ TPF(5)-269
F_06_06	6	4.26E+6	5.32E+2	6	4.79E+6	633	413	7.0	6.5
F_06_12	6	4.26E+6	5.32E+2	12	4.79E+6	602	387	9.3	7.0
F_07_06	7	4.26E+6	5.32E+2	6	4.79E+6	527	363	7.8	7.5
F_07_12	7	4.26E+6	5.32E+2	12	4.79E+6	505	343	10.0	7.9
F_08_06	8	4.26E+6	5.32E+2	6	4.79E+6	445	318	8.8	8.5
F_08_12	8	4.26E+6	5.32E+2	12	4.79E+6	429	303	10.7	8.8
F_09_06	9	4.26E+6	5.32E+2	6	4.79E+6	379	277	9.7	9.5
F_09_12	9	4.26E+6	5.32E+2	12	4.79E+6	367	267	11.5	9.8
F_10_06	10	4.26E+6	5.32E+2	6	4.79E+6	325	242	10.6	10.5
F_10_12	10	4.26E+6	5.32E+2	12	4.79E+6	315	234	12.3	10.8
F_11_06	11	4.26E+6	5.32E+2	6	4.79E+6	280	211	11.6	11.6
F_11_12	11	4.26E+6	5.32E+2	12	4.79E+6	273	205	13.1	11.8
F_12_06	12	4.26E+6	5.32E+2	6	4.79E+6	242	184	12.5	12.6
F_12_12	12	4.26E+6	5.32E+2	12	4.79E+6	237	179	13.9	12.8

2.4 Structural investigation of longitudinal cracking in rigid pavements

A finite element model was created to investigate the effect of a longitudinal crack in a slab on the stress distribution of an adjacent, loaded slab. Comparisons of the maximum stress were drawn between a set of slabs where one was either cracked or not cracked. A pavement section of two slabs over a subgrade with a modulus of subgrade reaction of 100 psi/in was made. Two slab panel sizes were investigated to explore any differences in stress from using wider slabs. A standard width slab with plan dimensions of 12 by 15 ft and a widened width slab of 14 by 15 ft were used. The 12 ft traffic lane was assumed to be off-centered on the widened width slab and shifted toward the centerline of the road. A 3 in. square mesh was used for the majority of the element sizes for the slabs modeled such that the simulated longitudinal crack could be uniformly centered within the element width. A plan view of the project basis for the simulations is shown in Figure 15.

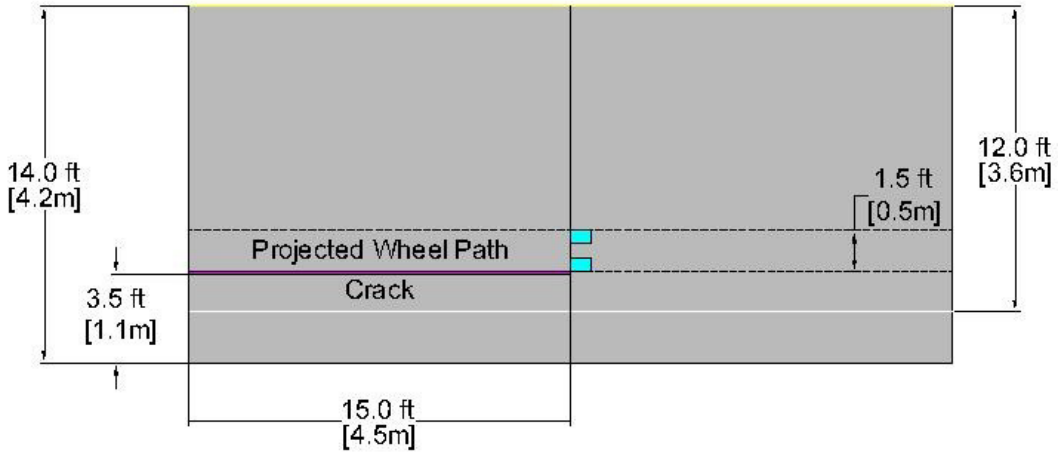

Figure 15. Location of existing longitudinal crack in two-slab simulations for stress response in vicinity of pre-existing longitudinal crack in a slab

The pavement was loaded with an axle and thermal load. A 9000 lb half axle equivalent single axle (dual tires) was used for the traffic loading in the analysis with the wheel load placed on the uncracked slab for analysis, as shown in Figure 15. A series of individual loading cases (factorial) was completed using different thermal loads. The linear thermal gradient through the slabs' cross-section was applied and ranged from 0 to 30°F in 10°F increments for the cases run. Only positive values for the thermal gradient were considered to investigate bottom-up longitudinal cracking. Negative gradients are associated with of top-down cracking and this particular method of cracking is not commonly observed. Additionally, load transfer efficiencies were varied for each load case modeled. Load transfer efficiency varied from 1% to 99.9% at intervals of 5%.

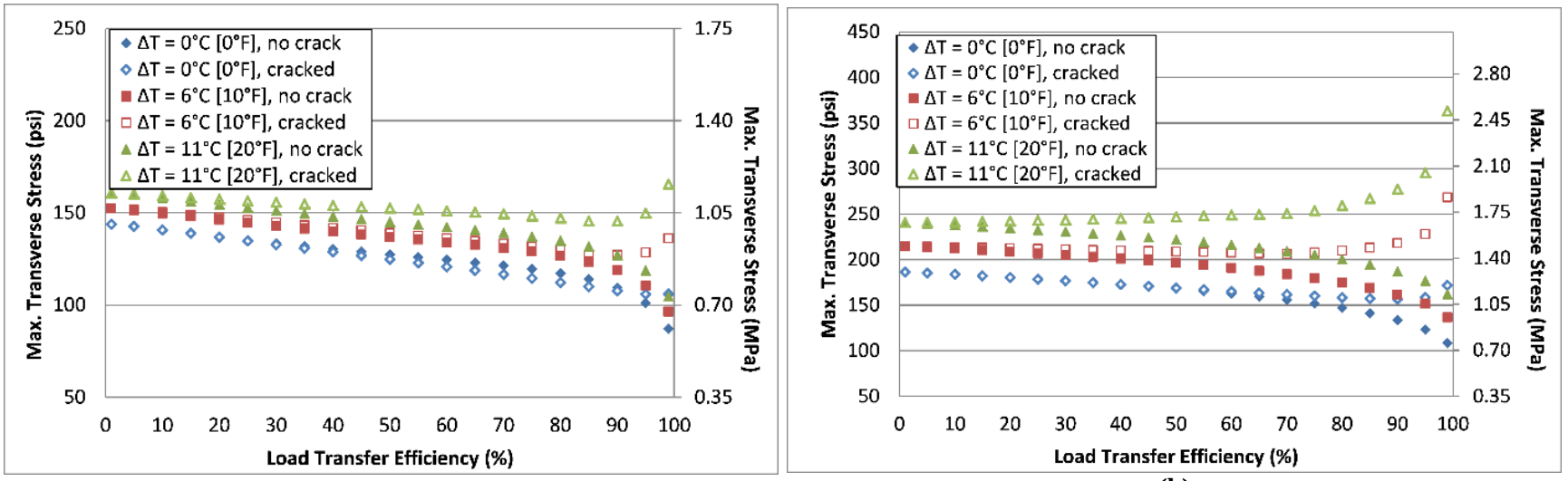

Figure 16. Computed maximum longitudinal stresses of the vehicle loaded slab for longitudinal crack simulation at the wheel path for varying load transfer efficiency and thermal load in (a) standard width slab and (b) widened slab

The simulation results in Figure 16 show that if an adjacent slab is cracked longitudinally, there is an increase in the stress in the loaded slab. Additionally, the benefits of load transfer between adjacent slabs are nullified or can begin to add stress to the uncracked loaded slab as the slab curls downward. The increased stress in the loaded slab can reduce the number of allowable load applications the pavement can withstand before failure from the increased stress and ultimately make propagation of the crack to undamaged adjacent slabs more likely. While the projected increase in stress is applicable and a concern in the standard width slab, the widened width cases are more interesting, as cracking is more likely to occur since the stresses are larger and yield a cumulative stress closer to the ultimate strength of the concrete.

In terms of design and construction of concrete overlays, the joint detailing of the pavement will have a significant effect on the stress distribution of the pavement. Undoweled joints rely on aggregate interlock to transfer load to surrounding slabs. Aggregate interlock load transfer is not as efficient in providing load transfer as a doweled joint and load transfer efficiency will generally be lower. Additionally, load transfer at aggregate interlock joints can be highly variable over time as the amount of contact between slabs changes, due to slab expansion and contraction with seasonal variations, and can reduce as the roughness of the crack breaks down. Stresses within the slabs will typically be higher with this joint type and lead to more favorable conditions for longitudinal cracking to initiate. However, once a cracked slab is created, stresses in adjacent slabs will continue to be approximately the same magnitude. Ultimately, lower values of load transfer efficiency would make stress estimation over the pavement's expected life easier to estimate since a common value could be used for the analysis period. This would not be true for a doweled joint based on the results of the investigation. The common practice of installing dowels to provide higher and more stable load transfer efficiency across joints will keep slab stresses lower initially and would either prevent or offset the time to cracking, since more load applications can be taken before cracking with lower stresses. However, once a crack does form, the dowels will fail to continue to reduce stresses in the slab and stresses will significantly increase since load transfer efficiencies will be towards the maximum value of 100%. Higher stresses can lead to propagation of the longitudinal crack to adjacent slabs and analysis methods would need to account for the stress distribution change for accurate predictions.

2.5 Evaluating the effect of cracks, joints, and voids on the structural response of unbonded systems

2.5.1 Effect of load and existing crack location on overlay response

As discussed in Sections 2.3.3 and 2.3.4, the Task 3 analysis simulations assumed unfavorable loading conditions for the structural models, wherein both A) a 18-kip single-axle load is applied directly over a crack at mid-slab in the existing slab and B) a thermal load is also applied to the system. These simulations can be expanded to answer other simple questions about the response of UBOL to loading. For this subsection, all simulations are conducted using a 6-inch overlay on a 9-inch existing slab, where all layer and mesh properties are identical to those of Section 2.3.3.

First, what if the load is not located directly over the crack in the existing slab? Figure 17 answers this question. As the load is moved away from the crack, the overlay response under load approaches the overlay response were the crack completely removed from the system.

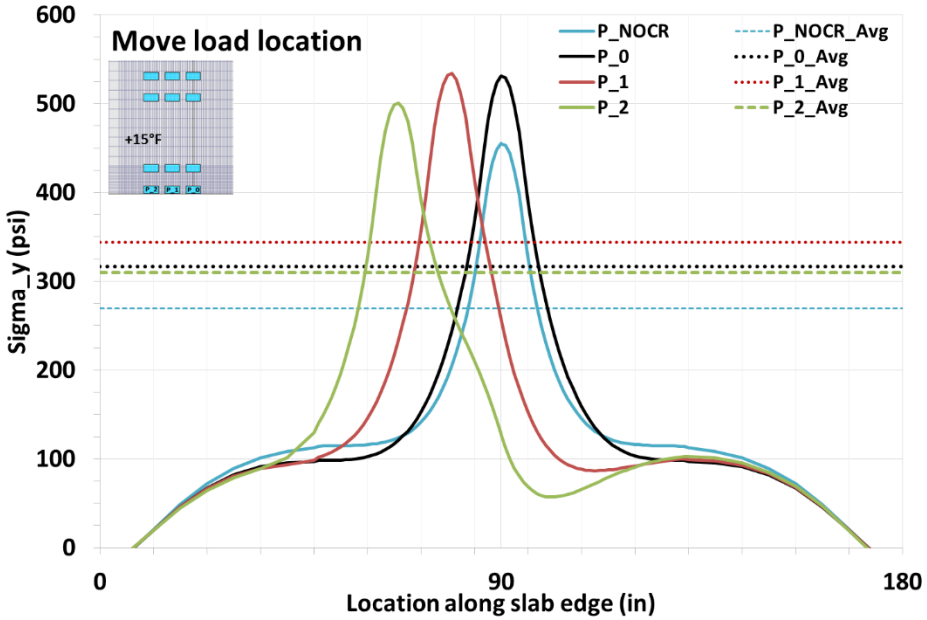

Figure 17. Four cases to evaluate stress response under load applied at different locations with stationary crack in existing PCC at mid-slab (includes "NOCR" case where crack in existing PCC is removed)

This first investigation in moving the applied load, however, can be made to more directly address the concern of estimating the condition of the existing slab and the effect of the condition on the performance of the slab. What if the crack were moved instead of the load? Figure 18 represents an attempt to answer this question. Note that as the location of the crack in the existing slab moves away from the load at mid-slab, the response of the overlay is nearly equivalent to the response of a UBOL system in which no crack is present.

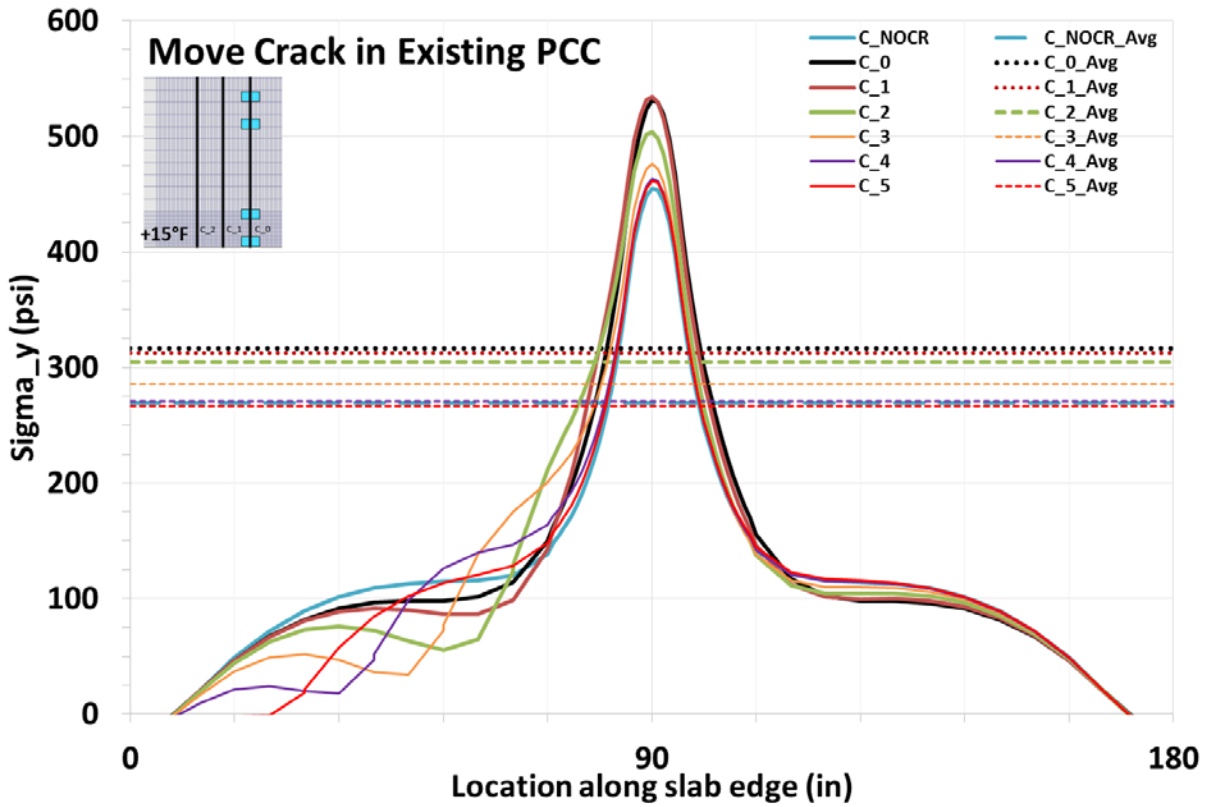

Figure 18. Six cases to evaluate stress response under load applied at mid-slab location with different locations for crack in existing PCC (includes "NOCR" case where crack in existing PCC is removed)

Using the six projects in Figure 18, which indicate the overlay response under load for cases when the crack is 0, 1, 2, 3, 4, and 5 feet from mid-slab, where the axle load is applied, one can roughly estimate an approximate region in which a crack in the existing slab significantly influences the overlay critical stress response. A summary of these projects is provided in Table 5.

Table 5. Overlay response under axle load at mid-span and thermal load for different crack locations in existing slab

Project	Crack Location (ft)	h_{OL} (in)	E_{OL} (psi)	k_{totsky}	h_{PCC} (in)	EPCC (psi)	σ_{max} (psi)	σ_{avg} (psi)
C_NOCR	--	6	4.26E+06	5.48E+03	9	4.79E+06	455.0	269.4
C_0	0	6	4.26E+06	5.48E+03	9	4.79E+06	531.1	316.7
C_1	1	6	4.26E+06	5.48E+03	9	4.79E+06	534.5	312.7
C_2	2	6	4.26E+06	5.48E+03	9	4.79E+06	504.0	304.8
C_3	3	6	4.26E+06	5.48E+03	9	4.79E+06	475.9	285.6
C_4	4	6	4.26E+06	5.48E+03	9	4.79E+06	463.2	270.7
C_5	5	6	4.26E+06	5.48E+03	9	4.79E+06	461.4	266.7

Evident in Table 5 is the idea that if the crack is sufficiently far enough from the load, the critical stress levels in the overlay quickly dissipate. Both Table 6 and Figure 19 are provided to make this result easier to observe.

Table 6. Overlay response under axle load at mid-span and thermal load for different crack locations in existing slab

Project	Crack Location (ft)	σ_{max} (psi)	σ_{avg} (psi)	Difference from NOCR		h_{eff} ISLAB TPF(5)-269 (in)
				σ_{max}	σ_{avg}	
C_NOCR	--	455.0	269.4	--	--	9.7
C_0	0	531.1	316.7	16.7%	17.6%	8.5
C_1	1	534.5	312.7	17.5%	16.1%	8.6
C_2	2	504.0	304.8	10.8%	13.1%	8.8
C_3	3	475.9	285.6	4.6%	6.0%	9.3
C_4	4	463.2	270.7	1.8%	0.5%	9.7
C_5	5	461.4	266.7	1.4%	-1.0%	9.8

If a crack in the existing slab exists three feet or more from the load at mid-span, σ_{max} will be increased by trivial levels (4.6% for the case when the crack is 3 feet from mid-span). On the other hand, if a crack exists two feet or less from the load at mid-slab, σ_{max} will be increased by 10 to 17 percent over its value were no crack present at all in the UBOL system.

This point can be reinforced by examining the equivalent structural performance of the system. When the crack is located four feet away from the load at mid-slab, the structural performance of the UBOL system as a single-layer composite is the same as its single-layer equivalent performance when no crack exists at all. Figure 19 reinforces this point through the manner in which the stress response at mid-slab for the different systems collapses to the “No Crack” case.

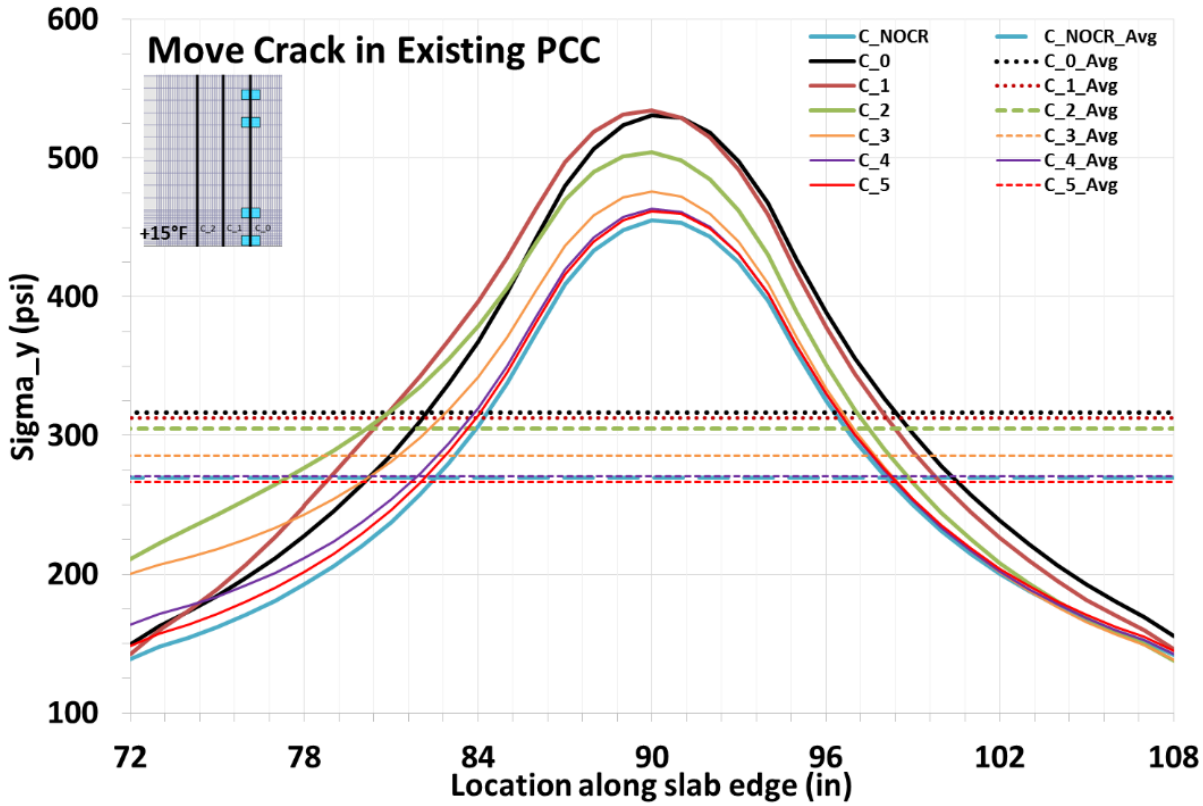

Figure 19. Local view (a three foot wide region centered on the load at mid-slab) for evaluation of response with different locations for crack in existing PCC

The project work will continue to investigate this issue in future tasks. By adequately estimating the likelihood of cracks in the existing slab that are near the critical mid-slab location in the overlay, the project UBOL design can be made to better estimate the structural performance of the system, which in turn will lead to improved performance prediction and thickness design.

2.5.2 Effect of interlayer deterioration at existing cracks in single-slab systems

An important consideration in UBOL systems is deterioration of the interlayer near joints and cracks. Using the finite element meshes created to evaluate the effect of existing PCC crack location on slab response, we can also include a 6-inch wide void in the interlayer, centered on the existing PCC crack, as a first investigation of the effects of degradation. Results of four simulations performed to investigate this are reported in Table 7 and Figure 20.

Additionally, the same meshes are used to investigate the effect of increasing the size of the void above an existing crack at mid-slab under load. One would expect that increasing the extent of interlayer degradation above an existing crack will exacerbate critical stresses even more. The results of these simulations, summarized in Figure 21, support this expectation.

Table 7. Overlay response under axle load at mid-span and thermal load for different crack locations in existing slab, with HMA interlayer void near existing crack (first 5 rows reproduced from Table 6)

Project	Crack Location (ft)	σ_{max} (psi)	σ_{avg} (psi)	Difference from NOCR		h_{eff} ISLAB TPF(5)-269 (in)
				σ_{max}	σ_{avg}	
C_NOCR	--	455	269	--	--	9.7
C_0	0	531	317	16.7%	17.6%	8.5
C_1	1	534	313	17.5%	16.1%	8.6
C_2	2	504	305	10.8%	13.1%	8.8
C_3	3	476	286	4.6%	6.0%	9.3
A_0_Cr	0 + Void	571	331	25.5%	22.7%	8.2
A_1_Cr	1 + Void	548	329	20.4%	22.0%	8.2
A_2_Cr	2 + Void	541	334	18.9%	24.1%	8.1
A_3_Cr	3 + Void	520	319	14.3%	18.2%	8.5

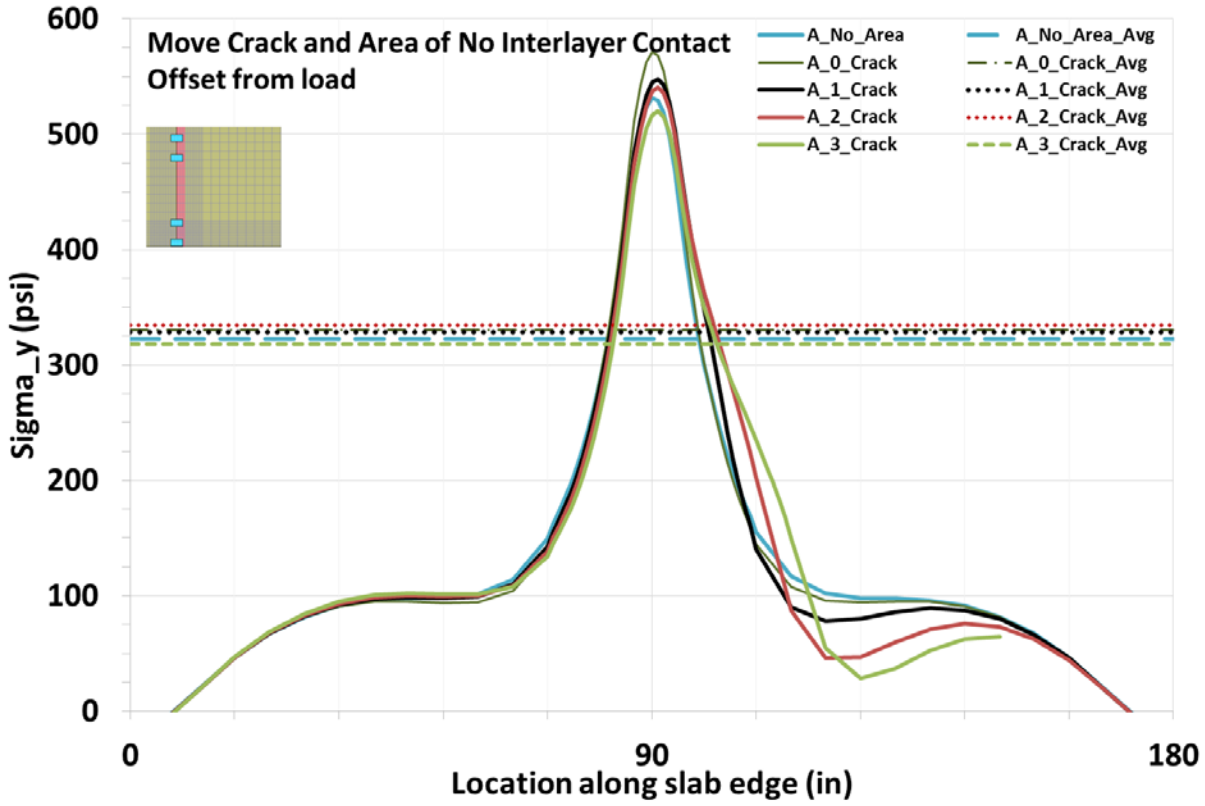

Figure 20. Four cases to evaluate stress response under load applied at mid-slab location directly over crack in existing PCC; cases distinguished by location of 6-inch wide void at the interlayer (includes "No_Area" case where void is removed)

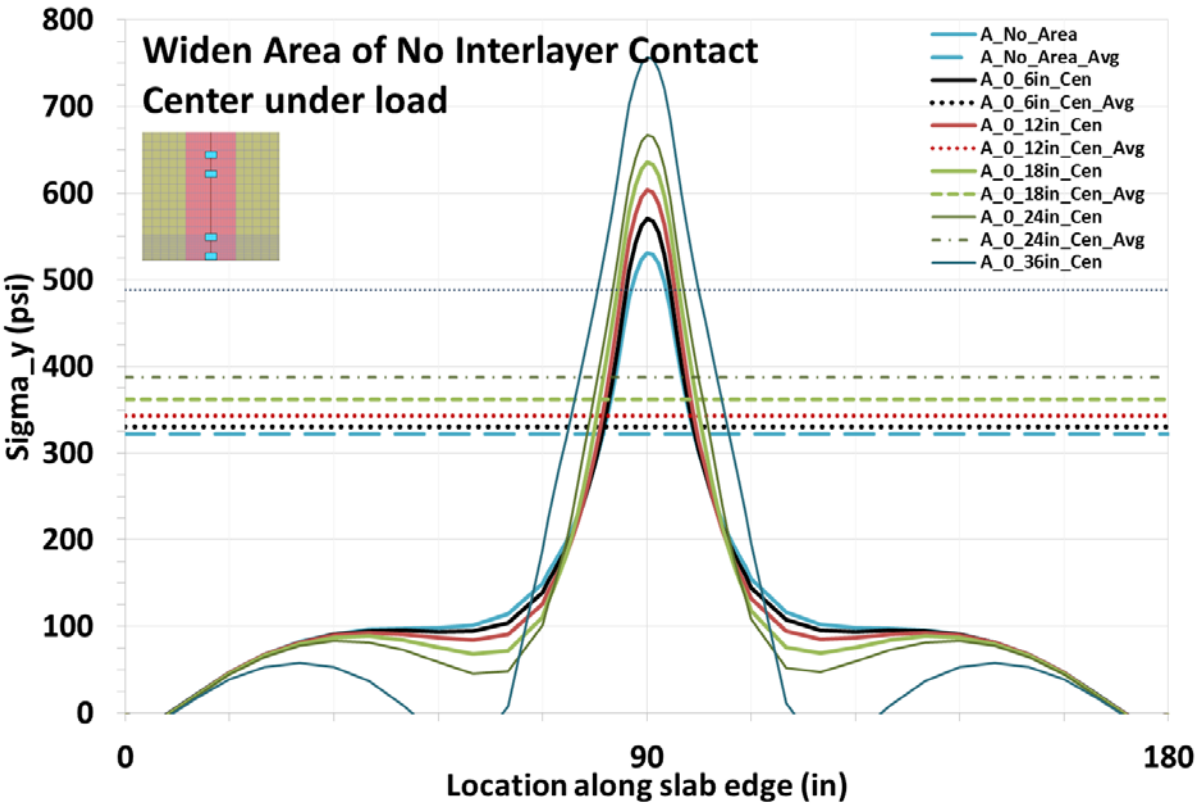

Figure 21. Six cases to evaluate stress response under load applied at mid-slab location directly over crack in existing PCC; cases distinguished by width of interlayer void centered on load (includes "No_Area" case where void is removed)

2.5.3 Effect of interlayer deterioration at joints in multiple-slab systems

A larger concern for UBOL systems, and rigid pavements in general, is deterioration at a joint between slabs/panels. To investigate joint deterioration, a new finite element mesh – shown in Figure 22 – was created. The mesh represents a system of two 12 foot by 15 foot slabs, jointed transversely. The mesh elements have dimensions of 6-inch on either side except for those elements within 18 inches of the joint. In that case mesh element are sized 1-inch along the dimension perpendicular to the joint.

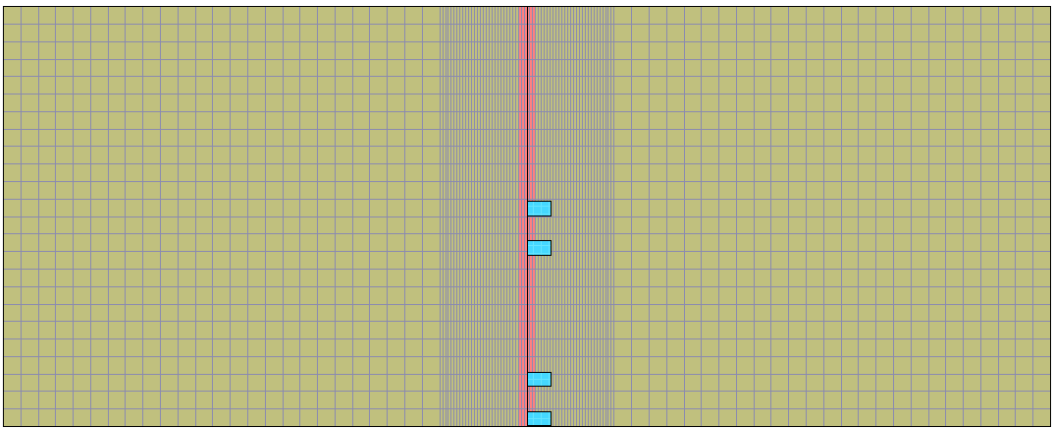

Figure 22. Mesh for investigation of effect of joint deterioration on two-slab system with 18-kip single axle load and positive and negative thermal gradients

The two-slab system in Figure 22 was used to create a total of 16 projects to understand the system response to wheel and thermal loading given variable joint LTE and variable width of deterioration under joint. Those projects have the following properties:

- A joint is assumed for Layer 1 with LTE of either 1% or 95%, whereas Layer 2 under the joint is assumed to be continuous (rigid).
- To simulate deterioration under the joint, a void of variable width is assumed in which the interlayer vertical stiffness is 0.1.
    - Assumed values for void widths are 0, 6, 12, and 18 inches.
- The overlay (Layer 1) has properties h_{OL} = 6 in, E_{OL} = 4,255,000 psi (average of all Task 2 beam overlay elastic moduli), Poisson ratio v = 0.15, and unit weight γ = 0.087 lb/in^3.
- The existing PCC (Layer 2) has properties h_{PCC} = 9 in, E_{PCC} = 4,790,000 psi (average of all Task 2 beam existing PCC elastic moduli), Poisson ratio v = 0.15, and unit weight γ = 0.087 lb/in^3.
    - The simulations assume Totsky approach for interlayer with vertical stiffness of 5478 (average of HMA interlayer values from Table 2).

The developed projects were subjected to two loading conditions:

- A standard 18-kip single-axle load with a positive 15°F linear thermal gradient through the thickness of Layer 1.
- A standard 18-kip single-axle load with a negative 15°F linear thermal gradient through the thickness of Layer 1.

Given that there are two critical stress locations (at the bottom of the overlay along the longitudinal edge and at the top of the overlay along the loaded side of the transverse joint), representing the stress fields along both locations for all 16 projects is difficult to read. Instead, an example of the stress response for a single case is shown in Figure 23 and Figure 24; in this case, there is no joint deterioration, the joint has an LTE value of 1%, and the thermal gradient is -15°F. Figure 23 presents the stress in the x-direction at the top of the overlay, whereas Figure 24

presents the stress in the y-direction at the bottom of the overlay. A summary of the maximum critical stresses in the overlay for the 16 projects is shown in Figure 25, where the location and stress direction are considered as before.

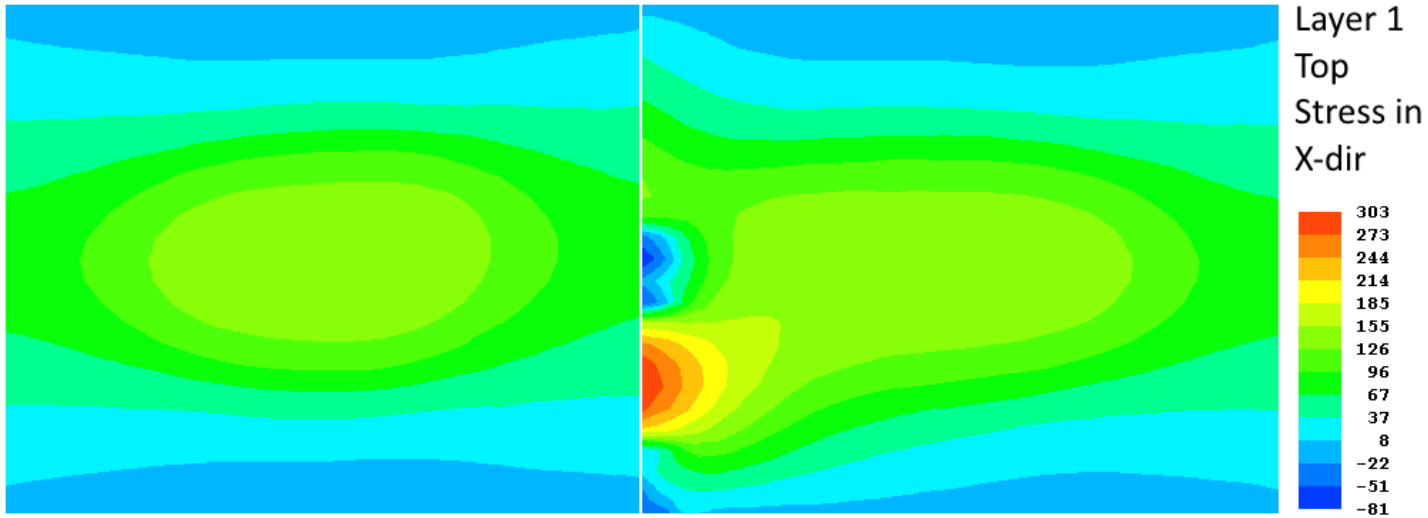

Figure 23. Example of overlay stress response in x-direction at top of jointed two-slab system; here there is no joint deterioration, 1% LTE, and negative thermal gradient (note scale for stress heat map, in psi)

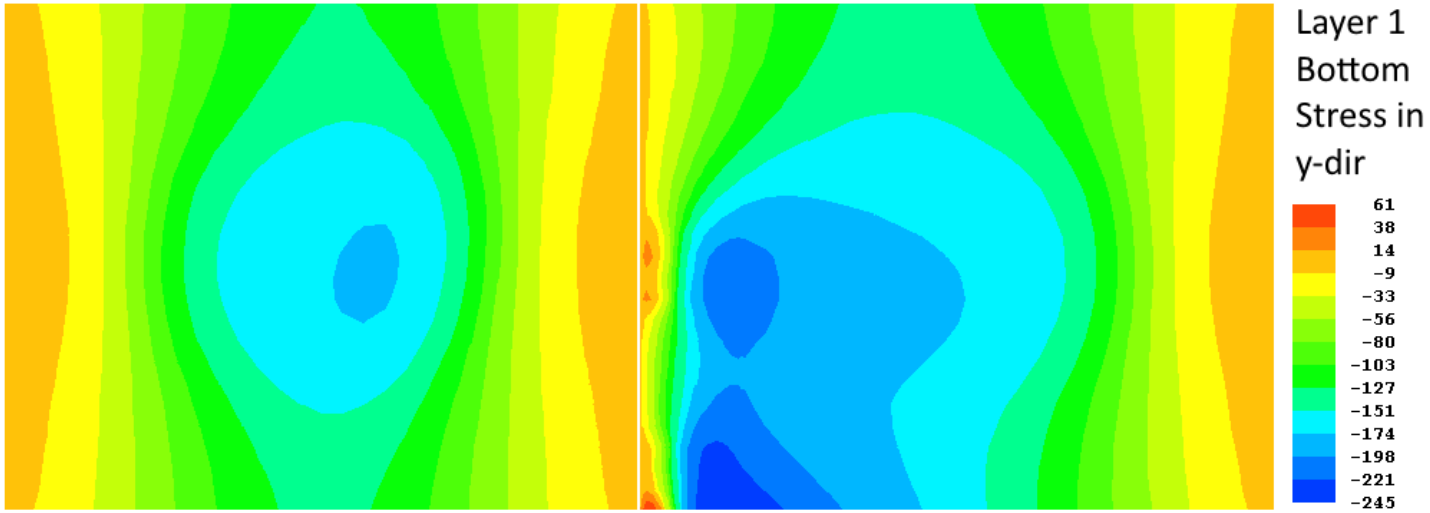

Figure 24. Example of overlay stress response in y-direction at bottom of jointed two-slab system; here there is no joint deterioration, 1% LTE, and negative thermal gradient (note scale for stress heat map, in psi)

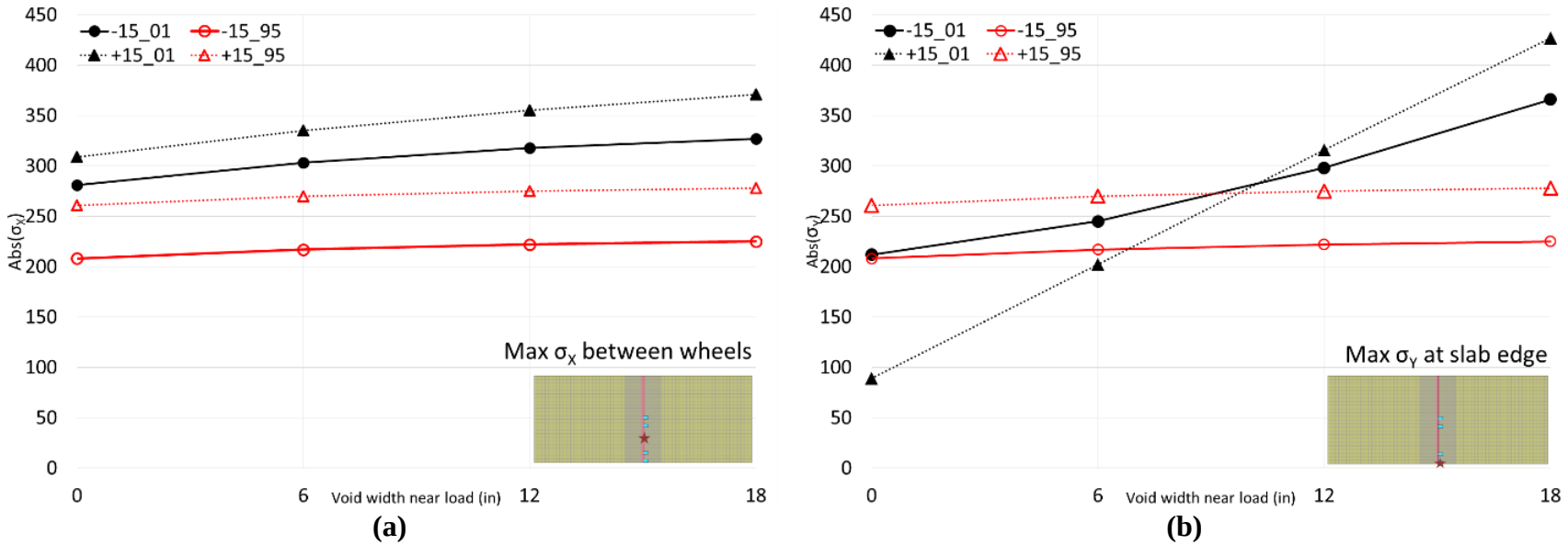

Figure 25. Effect of increasing area of deterioration under the joint on critical stresses (a) at mid-axle and (b) at slab edge

2.6 Case studies of six-foot UBOL panel response to wheel and thermal loading

While the research team did not conduct a formal factorial of finite element simulations for UBOL systems using six-foot panel, roughly 10-20 projects were created to compare the structural response of 6-foot-by-6-foot panels with more traditional 12-foot-by-15-foot slabs. Two meshes for an eight-panel system were created to serve as a basis for investigating the response of six-foot panels to wheel and thermal loading (Figure 26). One of the two meshes contains an existing PCC crack 6 inches from the applied load. The mesh elements have dimensions of 6 inches on either side except for those elements within 72 inches of the joint. In that case mesh elements are either sized 0.5 or 1 inches along the dimension perpendicular to the joint.

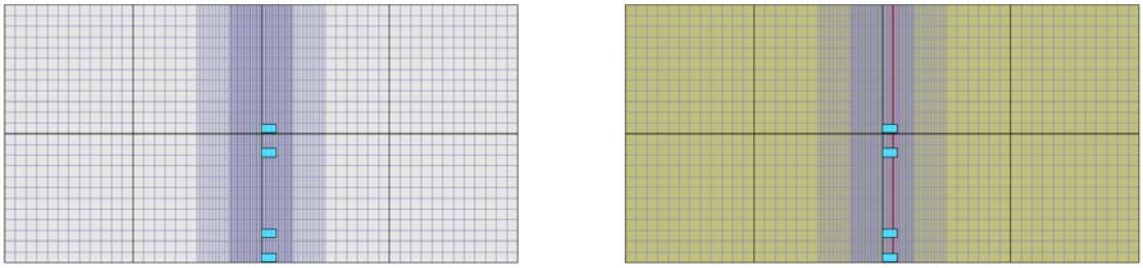

(a) (b)

Figure 26. Example meshes used for six-foot panel case studies include (a) a basic configuration of 8 panels and (b) including fictitious joints mid-panel to simulate existing cracks and voids to simulate deterioration near cracks

The six-foot panel projects developed using one of the two meshes have the following properties:

- The overlay (Layer 1) has properties h_{OL} = 6 in, E_{OL} = 4,255,000 psi (average of all Task 2 beam overlay elastic moduli), Poisson ratio ν = 0.15, and unit weight γ = 0.087 lb/in^3.
- The existing PCC (Layer 2) has properties h_{PCC} = 9 in, E_{PCC} = 4,790,000 psi (average of all Task 2 beam existing PCC elastic moduli), Poisson ratio ν = 0.15, and unit weight γ = 0.087 lb/in^3.
    - The simulations assume Totsky approach for interlayer with vertical stiffness of 5478 (average of HMA interlayer values from Table 2).

Additional properties assumed depend upon the case under evaluation. In general, the investigation attempted to replicate cases and conditions assumed for earlier projects 12-by-15-foot slabs. Assumed properties include a variable joint LTE for Layer 1 and/or a void of variable width is assumed in which the interlayer vertical stiffness is near zero. The developed projects were subjected to both wheel (standard 18-kip single-axle load) and/or thermal (linear thermal gradient through Layer 1) loading conditions.

Again, the research team did not conduct a formal factorial of simulations. Rather, given that the system-wide response of six-foot panels is not commonly simulated, six-foot panel projects were revised and iterated upon to understand their response more closely. This subsection will provide examples of some of these responses simply to illustrate this investigation – later project research may include a more focused approach to UBOL systems with six-foot panels if it benefits the project research. Figure 27 illustrates the deformation of

panels to a positive thermal gradient and single-axle loading. Figure 28 through Figure 31 provides heat maps of the stress response of the six-foot panels to wheel and thermal loading. Heat maps are used as A) there are two critical stress locations (at the longitudinal edge and at mid-axle) and B) the general response of six-foot panels is not often considered system-wide.

Overall, in comparing the six-foot panel systems to their 12-by-15-foot equivalents, it was found that the stress response was relatively similar, in part because the critical locations did not coincide with areas that are any more vulnerable in a six-foot panel than in a more conventionally sized slab. A major shortcoming of these simulations, however, is the loading conditions: future finite element simulations of these systems should include tandem and tridem axle loads.

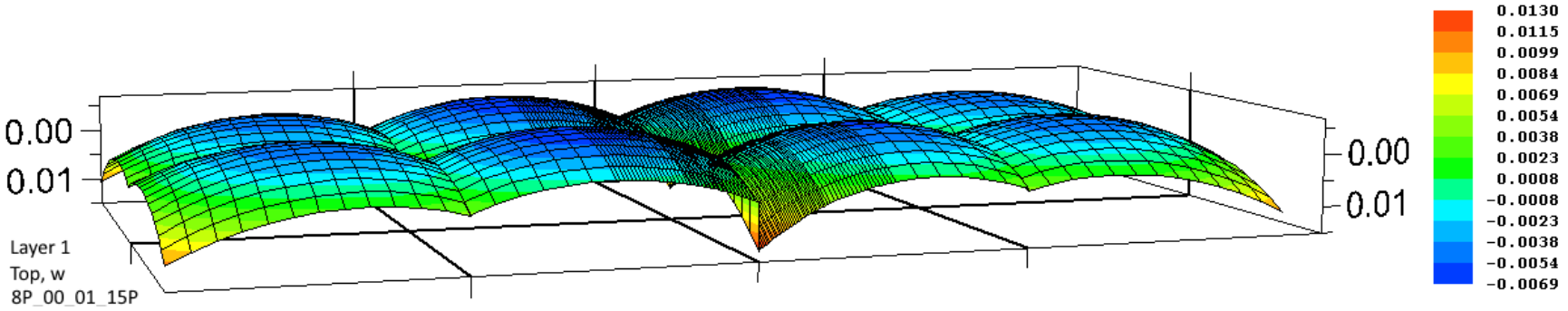

Figure 27. Example of deformed panels under a 15°F linear thermal gradient through overlay and an 18-kip single axle load

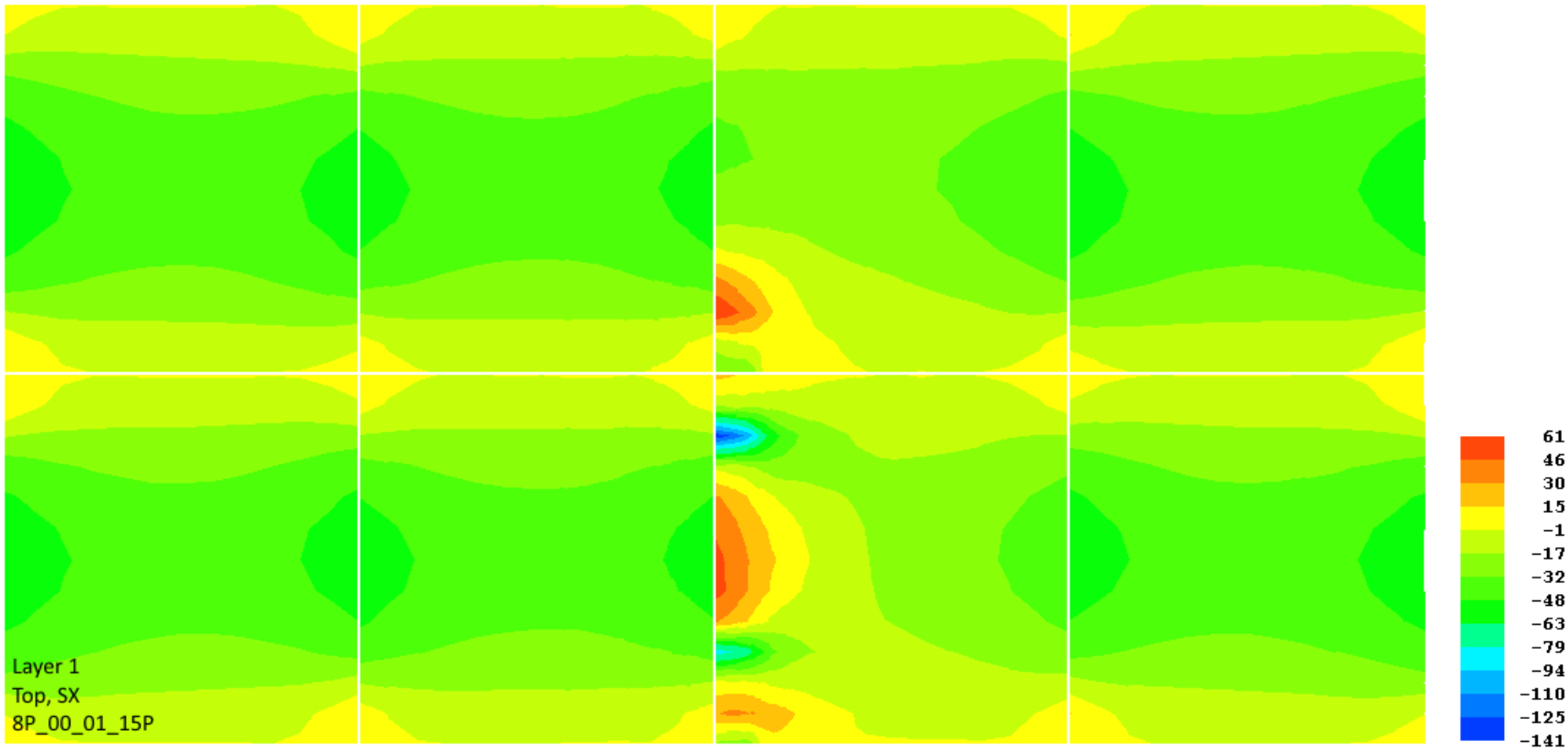

Figure 28. Example of stress response (in x-direction) at the top of the overlay under a 15°F linear thermal gradient through overlay and an 18-kip single axle load

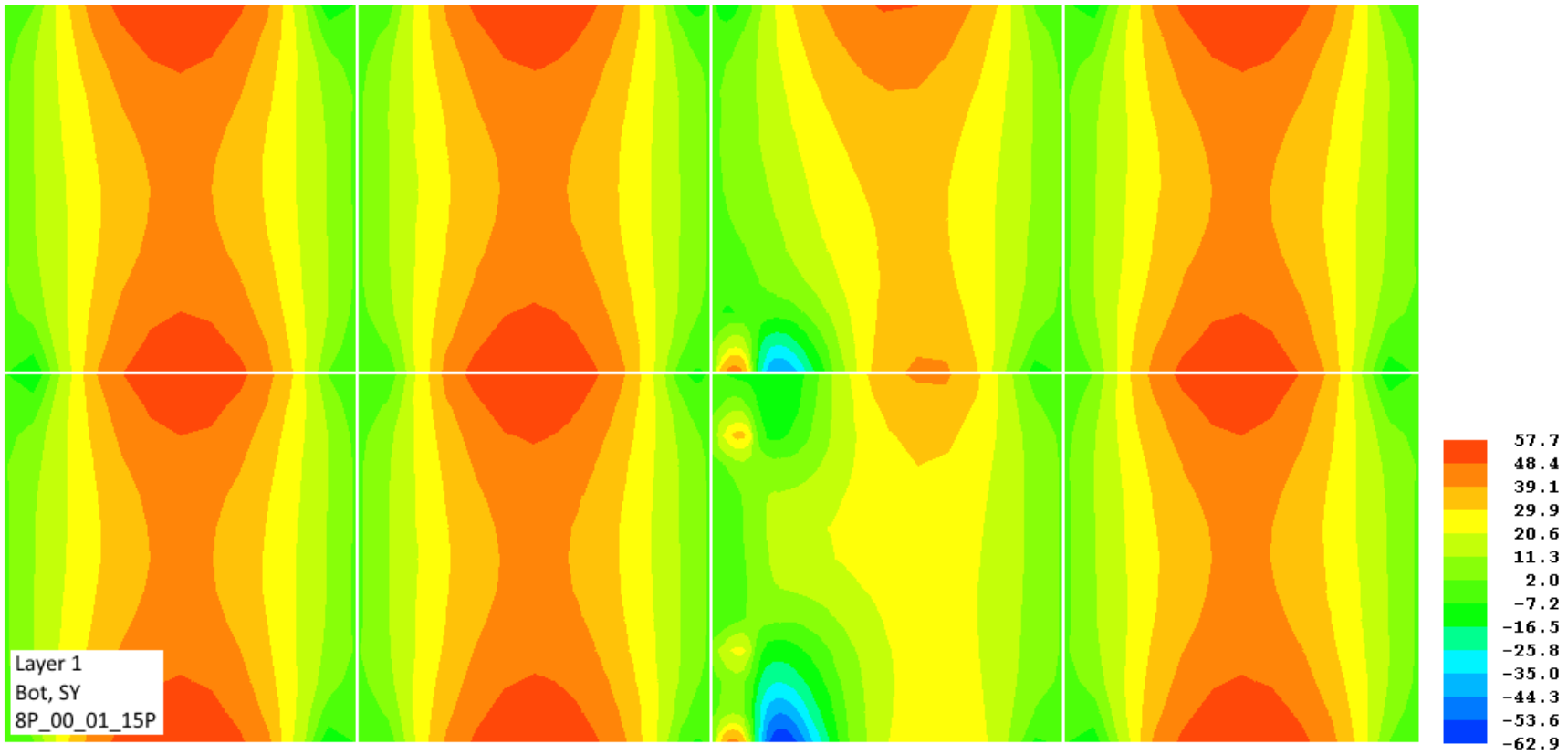

Figure 29. Example of stress response (in y-direction) at the bottom of the overlay under a 15°F linear thermal gradient through overlay and an 18-kip single axle load

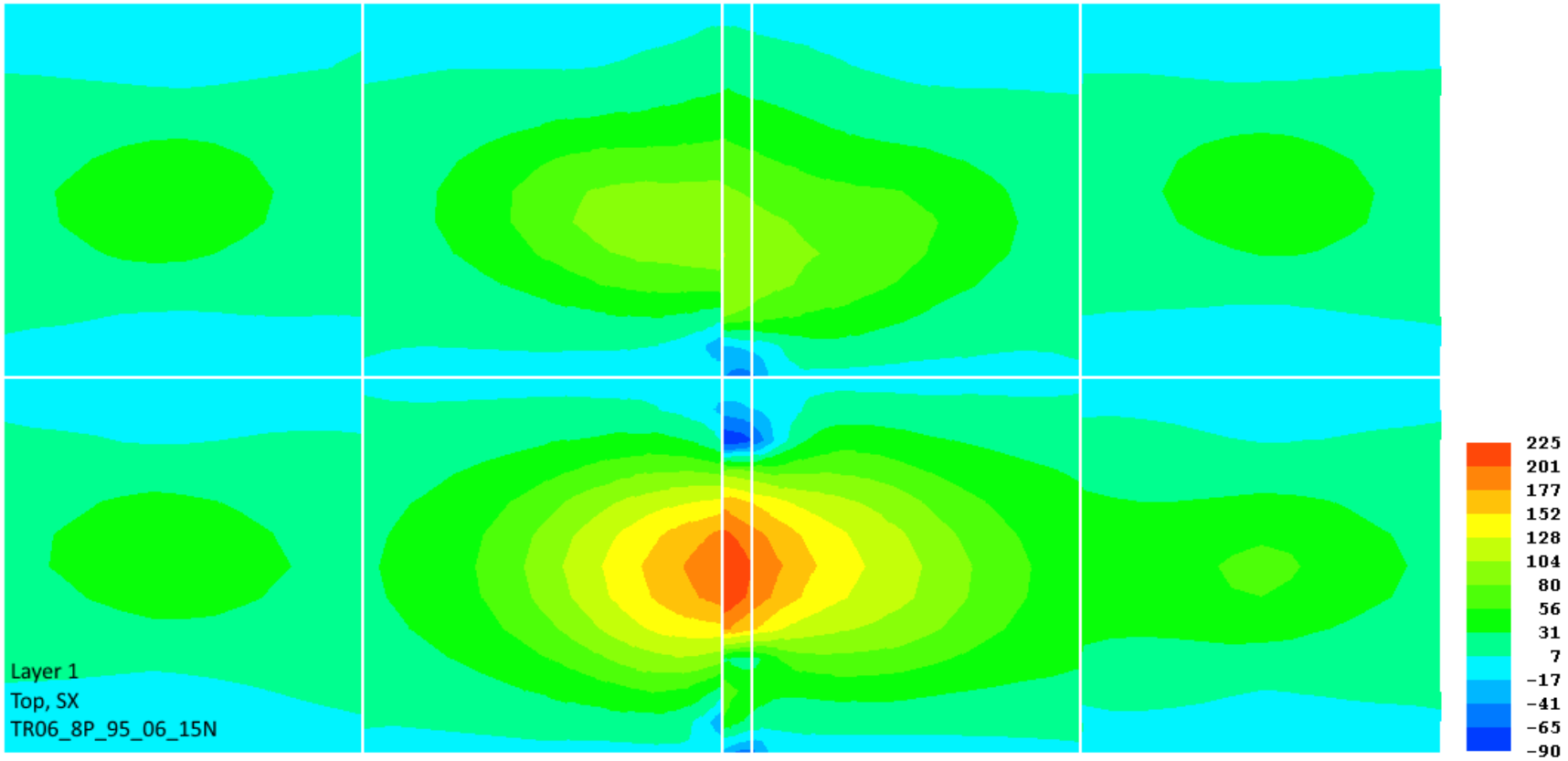

Figure 30. Example of stress response (in x-direction) at the top of the overlay near interlayer deterioration near an existing PCC crack for a pavement system under a negative thermal load and an 18-kip single axle wheel load

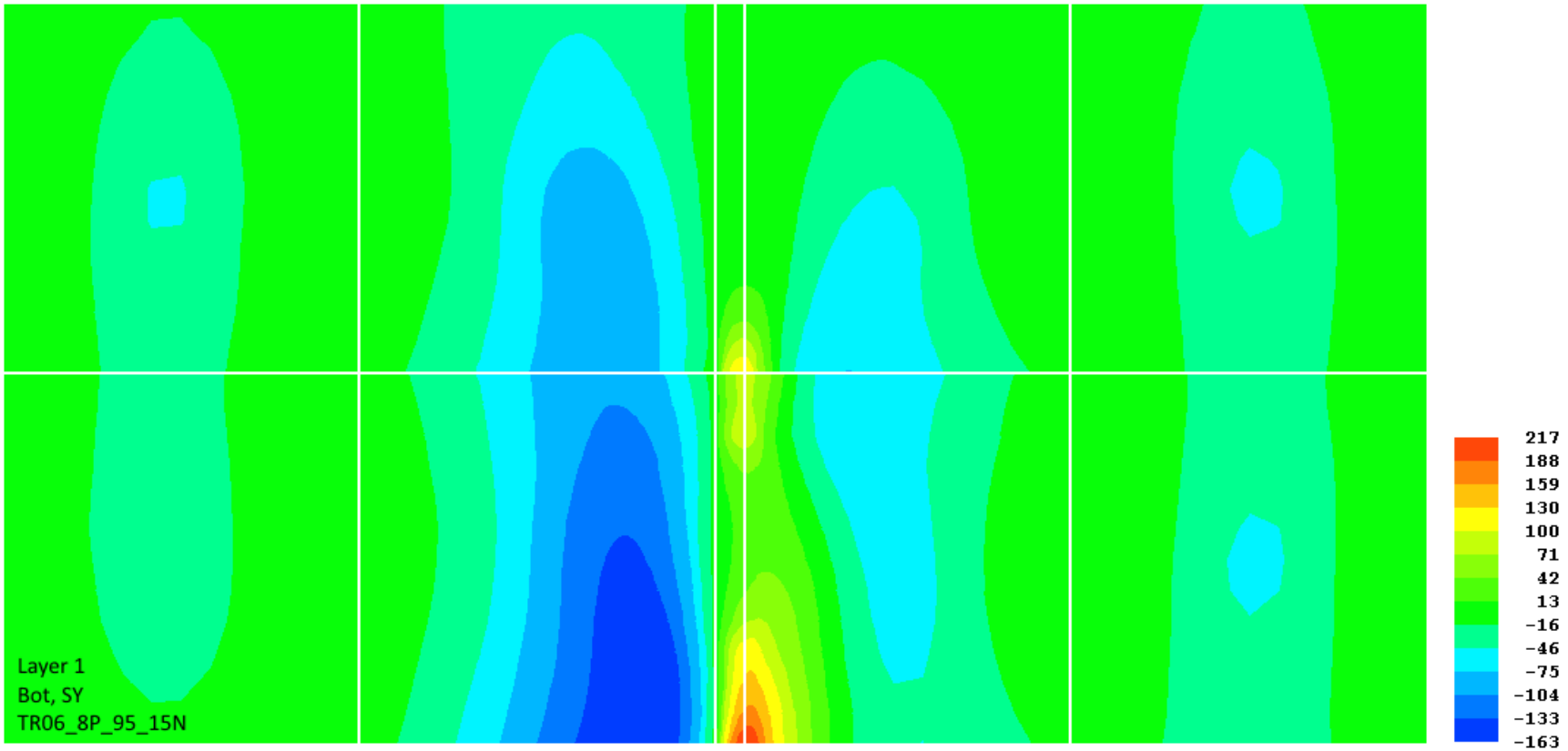

Figure 31. Example of stress response (in y-direction) at the bottom of the overlay near interlayer deterioration near an existing PCC crack for a pavement system under a negative thermal load and an 18-kip single axle wheel load

3. IMPLICATIONS OF STRUCTURAL MODELING ON PERFORMANCE MODELS FOR UNBONDED OVERLAYS OF CONCRETE PAVEMENTS

3.1 Transverse cracking

The structural model presented above in Section 2, which utilizes the Totsky approach for interlayer behavior, will replace the AASHTO M-E equivalent slab approach utilizing the Parallel Axis theorem. The proposed framework is compatible with the AASHTO M-E incremental damage approach to predict transverse cracking, and it can be combined either with a linear temperature gradient spectrum or an equivalent thermal approach developed in the work of TPF(5)-165, which led to the BCOA-ME software. An additional benefit of this model is that it can be used to provide a rational approach for the selection of the reduced stiffness of the existing pavement for the AASHTO M-E procedure if this is desirable.

At the same time, it was found that erosion of the interlayer can significantly affect top-down transverse cracking. Therefore, top-down cracking modeling should be combined with the joint faulting and interlayer erosion model using the AASHTO M-E incremental damage approach.

3.2 Longitudinal cracking

Longitudinal cracking in a slab/panel increases stresses in the adjacent slab, which accelerates longitudinal cracking development. Therefore, longitudinal cracking damage cannot be analyzed independently and later correlated with a percentage of cracked slabs as was done in the AASHTO M-E procedure for transverse cracking. In this study, the research team will address this problem by limiting longitudinal cracking damage, rather than quantifying longitudinal cracking directly.

3.3 Reflective cracking

In a past study using accelerated loading (Lederle et al, 2013), as well as the laboratory study of Task 2, the research team found that reflective cracking was difficult to produce in UBOL using the classical meaning of “reflective” (i.e. crack propagating upward by stress concentration due to cracking in existing pavement). At the same time, a reduction in the structural contribution of the existing pavement due to the presence of cracks can be accounted for directly, as was explained in discussion of the transverse cracking model. Therefore, no separate reflective cracking model for UBOL is necessary, and it will not be developed in this study.

3.4 Joint Faulting

An adequate joint faulting model for UBOL must address two issues: erodibility and permanent deformation. Understanding erodibility and the development of a void under a joint is a particularly pressing research need for this project. This understanding will be developed using a three-dimensional finite element model in ABAQUS. Whereas previous models and design procedures have touched on the issues of erodibility and permanent deformation indirectly, if at

all, the design procedure to be developed in this project must account for these issues directly. To this end, the research team has devoted extensive task effort to the development of a new joint faulting approach. This approach is summarized in the workflow of Figure 32.

The faulting approach summarized in Figure 32 considers four different modes of damage: faulting, fatigue, erosion, and consolidation. When examining erosion and faulting, it will be necessary to consider the effects of traffic, moisture (climate), asphalt susceptibility, and drainage. Parameters to be extracted from the model include the peak deflection directly under the overlay slab (loaded and unloaded sides of the joint) and the sum of the basin deflection in a 3 ft grid around the overlay joint. Neural networks will then be developed for these critical parameters based upon the modeling inputs. Additionally, an interlayer erodibility factor will be developed which considers if water is draining through the interlayer, the mixture design, binder content, film thickness, and permeability. The erodibility factor and the predicted critical response from the neural networks will be used to predict an erosion depth within the interlayer. This erosion depth will then feed into the faulting prediction algorithm.

Consolidation and fatigue are a function of traffic, asphalt compressive strength, vertical interlayer strain, load transfer efficiency, and deflection. Parameters to be extracted from the model include the peak vertical strain in the interlayer, the vertical strain in the interlayer in a 3 ft region around the joint in the overlay, the peak tensile strain at the bottom of the interlayer, and the peak deflection directly under the overlay slab (loaded and unloaded sides of the joint). Neural networks will also be developed for these critical responses. Fatigue can be accounted for by applying a Miner's hypothesis approach looking at the peak vertical strain at the top of the interlayer and the peak tensile strain at the bottom of the interlayer and comparing these with strains at failure. This value of predicted damage will feed into the faulting prediction algorithm in conjunction with the predicted erosion depth. The critical parameters for consolidation can be used to predict voids that may develop between the interlayer and the overlay. This void contributes to the development of longitudinal cracking in the wheelpath. The faulting model will only consider asphalt interlayers since faulting cannot develop within a fabric interlayer.

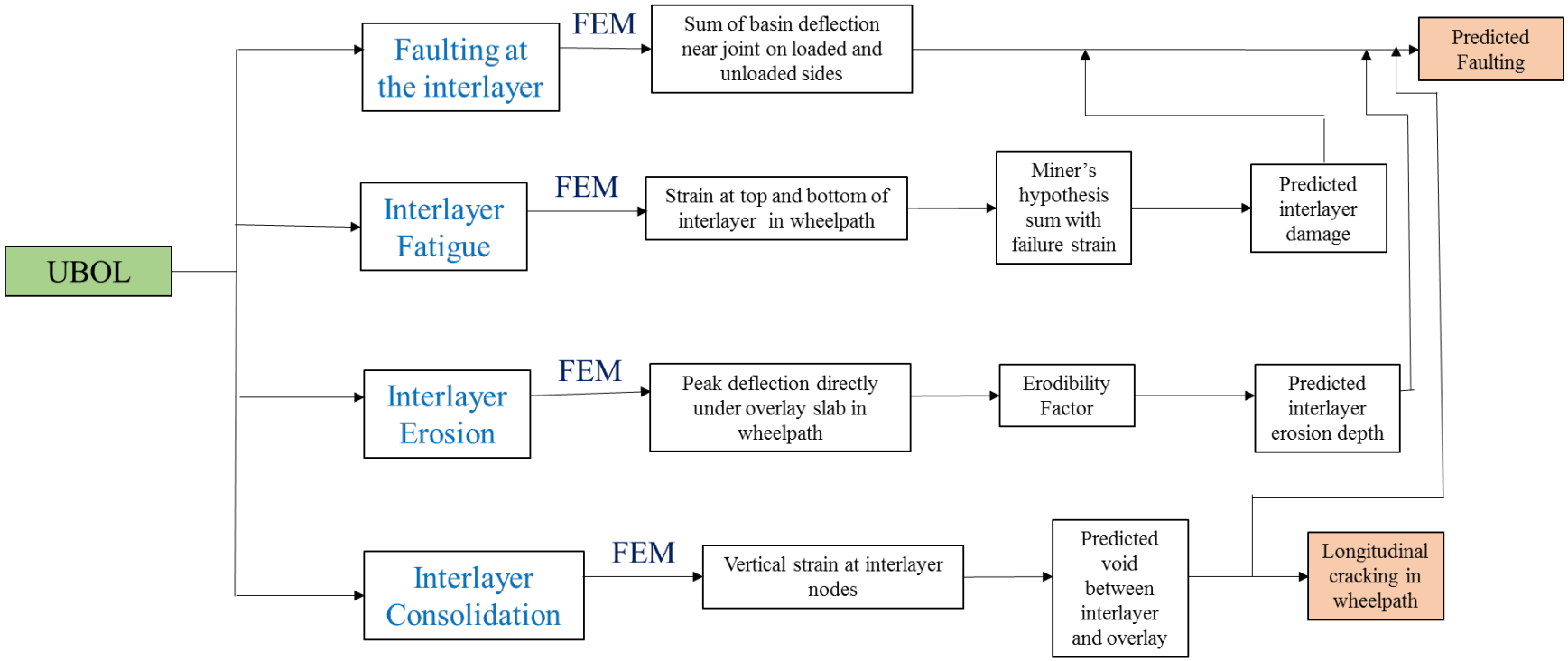

Figure 32. Framework for faulting prediction

3.4.1 Three-dimensional finite element model for UBOL faulting response

3D modeling of the pavement structure will be carried out using the general purpose finite element code ABAQUS. Figure 33a shows the model with all relevant dimensions, while Figure 33b provides an example of a mesh used for simulations conducted for this effort.

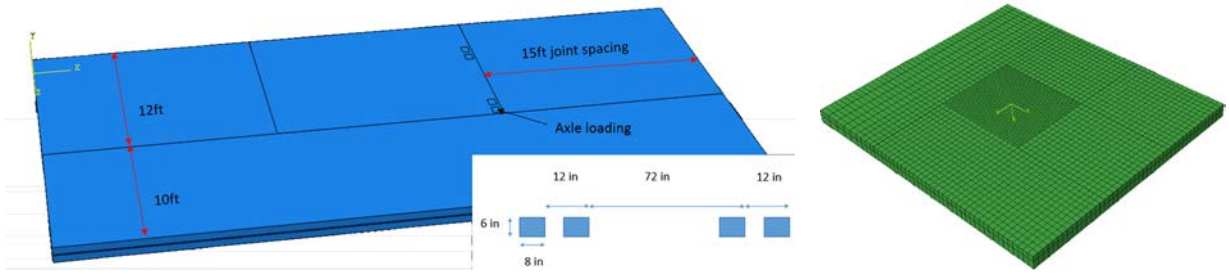

(a) **(b)**

Figure 33. (a) Schematic of proposed model for faulting response and (b) finite element mesh used for a 6-by-6 foot panel configuration

Three overlay slabs, a shoulder, an interlayer and the existing PCC will be modeled. Overlay joint spacing will include 10, 15, and 20 ft with a 12 ft lane width. Six by six ft slabs will also be modeled as can be seen in Figure 34. The shoulder width will be 10 ft. A tire footprint of 6 x 8 in will be used along with the axle and dual tire spacing dimensions shown in Figure 33a (inset).

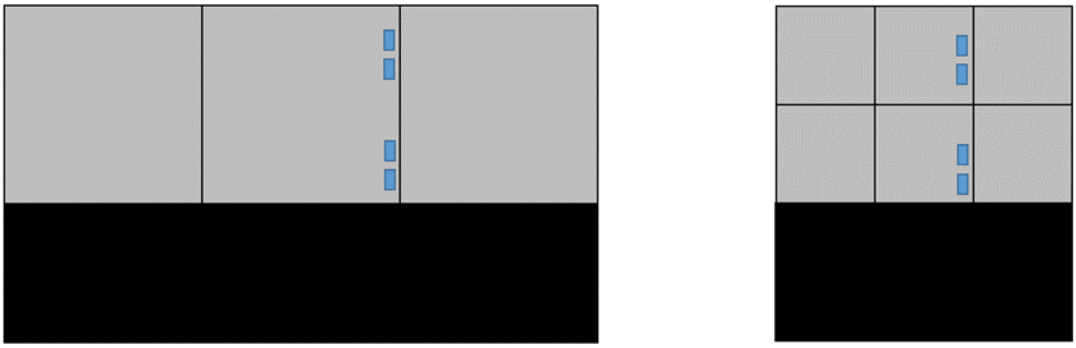

(a) **(b)**

Figure 34. Plan view of slab configurations in the (a) 10, 15, 20 ft joint spacing model and (b) 6-by-6 ft panel model for three-dimensional modeling for faulting response

The model accounts for parameters summarized in Figure 35 and discussed below.

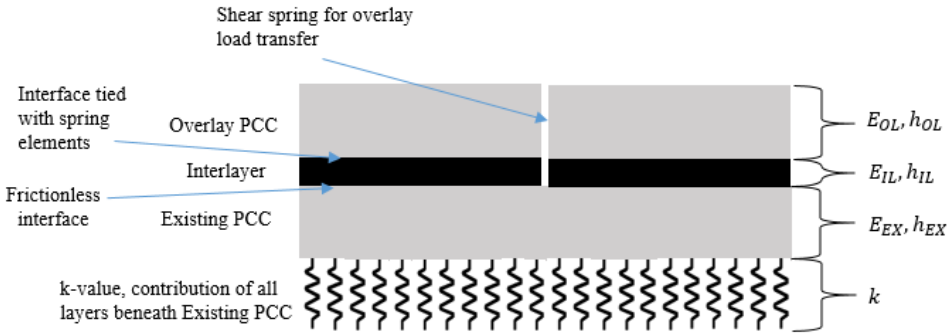

Figure 35. Layer properties considered in three-dimensional faulting model

PCC and asphalt layers. The overlay and existing PCC and the asphalt interlayer are modeled as elastic solids with an elastic modulus and Poisson ratio. A Poisson ratio of 0.18 and 0.35 are used for PCC and asphalt respectively. The elastic moduli of the layers will vary within the factorial of runs. Isotropic linear expansion was also given to all three layers. The values of linear expansion for the PCC will vary, and a value of 6*10-6 in/in/oF was assigned to the asphalt. Currently, 20 node brick elements (C3D20) are used to model the PCC and asphalt layers.

Foundation Support. The composite behavior of all layers beneath the existing PCC layer is represented as a Winkler foundation. The bottom surface of the existing concrete is to be defined as an "Elastic foundation" interaction in the initial step which is propagated into the load steps.

Transverse Joints. Load transfer across the joints is being employed with shear springs which have only degrees of freedom in the y-direction in the model. The springs are attached to both the approach and leave faces of the joint at the nodal of the elements. Three spring constants will be used at different locations at the joint to represent the different stiffness. K will be used at the corner nodes, 2K for the edge nodes, and 4K for the interior nodes. "Hard Contact" interaction is applied at the two faces on the joint. The effects of both aggregate interlock and doweled joints will be considered at these joints. The approach used to account for these two contributions to load transfer will follow a similar methodology to Pavement ME (ARA 2004). The joint through the overlay will also extend through the interlayer, however no load transfer will be simulated through the interlayer. If 3 values of spring stiffness at the joints are used for the generation of input parameters, then 3 values of load transfer will be achieved ranging from just load transfer of the existing structure slab to 100 percent load transfer efficiency.

Longitudinal Joints. The lane shoulder joint will be modeled as either an asphalt shoulder or a tied PCC shoulder. No load transfer through the asphalt shoulder will be modeled, while a tied lane shoulder joint will be modeled with a load transfer of approximately 90 percent. The longitudinal joint which must be modeled for the 6 x 6 ft slabs will only provide shear transfer at a level less than the transverse joint if dowels are to be considered for the transverse joints.

Interface bond. Only an asphalt interlayer will be modeled since faulting cannot develop in a fabric interlayer. The bond between the overlay PCC and asphalt interlayer is modeled as fully

bonded when the interlayer is an elastic solid. This is achieved with the springs connecting nodes with a large spring constant of 2,000,000 lb/in. The interface between the existing PCC and the interlayer will be modeled as "frictionless" creating full slip between the two surfaces.

Wheel and thermal loads. A gravity load is applied in the "General, static" step 1 and is treated as a uniform pressure on the surface of the pavement equal to the weight of the structure. An axle load is applied at one side of the joint as shown in Figure 34 and is applied in the "General, static" load step 1. The effects of wheel wander, axle type (single, tandem, tridem), and load magnitude will be accounted for within a fractional factorial to encompass an unbiased subset of the total number of finite element runs to perform. Temperature gradients will be treated as a "Predefined Field" temperature load at the surfaces of the PCC. Uniform distributed temperature loads will be applied to both the top and the bottom of the PCC layer to induce a linear variation in temperature from the top to the bottom of the PCC layer. Nonlinear temperature differences based upon the equivalent strain concept will be employed.

3.4.2 Proposed structural and load parameters considered in three-dimensional faulting model

In order to decrease the number of finite element runs required, some parameters within the structure have been combined with one another. This can be seen in Figure 36. The values of the existing thickness, stiffness, and k-value can be combined into a radius of relative stiffness. The radius of relative stiffness can be adjusted from 20, 35, 50, 65, and 80 in by leaving the stiffness of the existing concrete as 4,500,000 psi and the k-value as 100 psi/in and only adjusting the thickness. The range of existing thicknesses becomes 3.5 to 22 in to further decrease the number of finite elements runs to generate only different values of flexural stiffness for the PCC overlay. The overlay elastic modulus can remain 4,000,000 psi and only the thickness be increased. The values of overlay flexural stiffness could be $2*10^7$, $2.4*10^8$, $4.6*10^8$, $6.8*10^8$, $9*10^8$ lb-in; these values correspond with overlay thicknesses between 3.9 and 13.8 in.

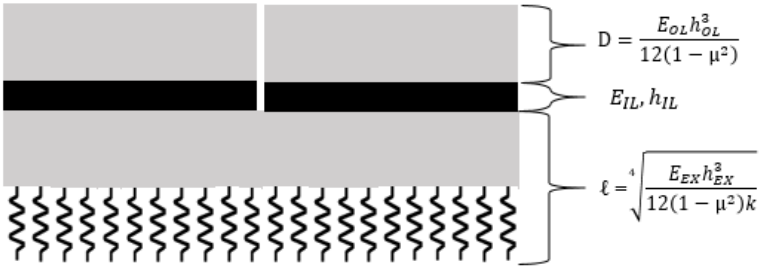

Figure 36. Consolidation of structural parameters for faulting model

These parameters and values in addition to all the remaining parameters can be seen in Table 8. As previously stated, the Poisson's ratio of the PCC and asphalt will be 0.18 and 0.35 respectively along with 6, 10, 15, and 20 ft joint spacing. Also, both an asphalt and tied shoulder will be simulated. Two different coefficients of thermal expansion (CTE) and three linear temperature differences of the top minus the bottom will be modeled. The interlayer thickness will be modeled as 2 in and will be simulated with four different elastic moduli. Finally, the combination of axle loading and wheel wander will be accounted for with a factorial subset of combinations to minimize the number of finite element runs necessary.

Table 8. Proposed variation in parameters in the three-dimensional faulting model

Parameter	Range				
Existing slab and foundation, l (in)	20	35	50	65	80
PCC Poisson's ratio	0.18				
Overlay Flexural Stiffness, D (#-in)	2.00E+07	2.40E+08	4.60E+08	6.80E+07	9.00E+08
Overlay PCC jt spacing (ft)	6	10	15	20	
Overlay PCC CTE (in/in/^{o}F)	3.80E-06	5.50E-06			
Overlay Temp Difference (^{o}F)	-12	0	24		
Interlayer Thickness (in)	2				
Interlayer Stiffness (psi)	100000	400000	700000	1000000	
Interlayer Poisson's ratio	0.35				
Interlayer CTE (in/in/^{o}F)	6E-06				
Lane shoulder LTE (%)	Tied PCC	Asphalt			
Wheel wander (in)	0	2	6	12	36
Single axle (lb) Tandem axle (lb) Tridem axle (lb)	0-45,000 (15 kip increment) 0-90,000 (30 kip increment) 0-120,000 (40 kip increment)			Fractional Factorial	

REFERENCES

ABAQUS (2011). ABAQUS Theory Manual (6.11).

Applied Research Associates (ARA), Inc., ERES Division (2004). *Guide for Mechanistic-Empirical Design of New and Rehabilitated Pavement Structures*. Final Report NCHRP 1-37A. Transportation Research Board of the National Academies, Washington, D.C., 2.4.26.

Lederle, R., Hoegh, K., Burnham, T. and L. Khazanovich (2013). Drainage Capabilities of a Nonwoven Fabric Interlayer in an Unbonded Concrete Overlay (13-4107). *Proceedings of the 92nd Annual Meeting of the Transportation Research Board*, Washington, D.C., January 13-17, 2013, Transportation Research Board, National Academy of the Sciences, Washington, D.C.